

A Chronicle About the Development of Electronic Structure Theories for Transition Metal Complexes

Tom Ziegler

Abstract We review here the development of electronic structure theories for transition metal complexes from the 1950s to present days. The different methods are compared through applications to permanganate and other tetroxo systems.

Keywords Constricted density functional theory · Density functional theory · Electronic structure theory · Hartree–Fock method · Post-Hartree–Fock methods · Time-dependent density functional theory

Contents

1	Introduction	2
2	Ground State Electronic Structure Theory	3
2.1	The Hartree–Fock Method	3
2.2	Density Functional Theory and the Kohn–Sham Equation	7
2.3	Post-Hartree–Fock Methods	12
2.4	Applications to the Ground State of Permanganate and Related Tetroxo Systems ..	13
3	Excited State Electronic Structure Theory	18
3.1	Different DFT-Based Methods Used in the Study of Excited States	18
3.2	Different Hartree–Fock and Post-Hartree–Fock Methods Used in the Study of Excited States	27
3.3	Theoretical Studies on the Absorption Spectrum of Permanganate and Related Tetroxo Complexes	28
3.4	Theoretical Studies on the Magnetic Circular Dichroism Spectrum of Permanganate and Related Tetroxo Complexes	31
4	Concluding Remarks	33
	References	34

1 Introduction

The formulation of an electron structure theory for coordination compounds containing transition metals began shortly after the introduction of quantum mechanics with the development by Becquerel [1], Bethe [2] and Van Vleck [3] of crystal-field theory. A giant step forward was taken in the 1950s by the development of ligand field theory [4, 5] that combines the ideas of crystal field theory with those of molecular orbital theory [6] and allows for an elegant interpretation of the spectra of coordination complexes. C. J. Ballhausen was one of the pioneers in this development and his book on ligand field theory from 1962 [5] influenced a whole generation of coordination chemists.

Ballhausen started his carrier in the lab of J. Bjerrum at the University of Copenhagen in the early 1950s. This was an environment that continued the strong Danish tradition in coordination chemistry dating back to S.M. Sørensen and N. Bjerrum. At the time (1950), the lab attracted several international visitors including F.A. Cotton and F. Basolo. It testifies to the strength of the group that it fostered two other young members that went on to contribute significantly to ligand field theory, namely C.E. Schäffer and C. K. Jørgensen. The theoretical interest by the three young members of the Bjerrum team was very much whetted by the appearance in 1951 of a paper [7] due to F.E. Ilse and H. Hartmann in which the two authors explained the electronic spectrum of the $\text{Ti}(+3)$ ion based on crystal field theory.

After establishing his own lab, Ballhausen began in the 1960s on a research program that combined high-resolution spectroscopic measurements with interpretations based on theoretical methods. These methods included not only ligand field theory but increasingly also other schemes based on Roothaan's formulation [8, 9] of molecular orbitals theory as they emerged in the 1960s and 1970s. Ballhausen would not take directly part in the development of these new methods but he encouraged people in his lab to do so. This encouragement was also extended to young students such as myself. Thus when I started as a M.Sc. student in the Ballhausen lab (1969), I was given the task to evaluate semi-empirical methods that were applied to transition metals at the time and possibly come up with improvements. I was very fortunate to be introduced to the electronic structure theory of transition metal complexes at a time when the field was undergoing a revolution [10]. Thus although I soon lost all interest in semi-empirical methods, my time with Ballhausen and his collaborator J.P. Dahl launched a lifelong interest in transition metal complexes and methods that could describe their electronic structure. It is the objective of this account to chronicle some of the highlights from the early beginnings of theoretical transition metal chemistry in the 1950s to present days powerful electronic structure theories.

In the period (1969–1972) when I was a student with Ballhausen, his lab was an international center with visitors from many different parts of the world representing a multitude of different research interest. One particular subject that caught my interest was the electronic structure and absorption spectrum of

permanganate and related tetroxo complexes. The electronic spectrum of permanganate was first studied by Teltow [11] in 1938. However, with modern techniques Holt and Balhausen [12] had in 1967 recorded a high resolution low temperature absorption spectrum of MnO_4^- . Shortly after, attempts were made to assign the observed spectrum with any available computational method. It was felt that permanganate as a small system with a pleasingly high symmetry should be an easy task for theory. The implication here was that if theory cannot treat as simple a system as MnO_4^- , it would appear not to be of much use at all. As we shall see, the notion of permanganate being an easy system is completely wrong. In fact permanganate is one of the most difficult electronic systems to describe. We shall demonstrate this through a number of applications to MnO_4^- that are used to gauge the ability of the different theories chronicled in this account.

2 Ground State Electronic Structure Theory

We shall in this section give a historic overview of how the electronic structure theory for transition metal complexes in their ground state has evolved from the 1950s to the present time. The account will include a discussion of wave function methods based on Hartree Fock and post-Hartree Fock approaches as well as Kohn–Sham density functional theory (KS-DFT).

2.1 The Hartree–Fock Method

In Hartree–Fock theory, we approximate the many-electron wave function with a single Slater determinant

$$\Psi = \frac{1}{\sqrt{N!}} \begin{vmatrix} \psi_1(x_1) & \psi_2(x_2) & \dots & \psi_1(x_N) \\ \psi_2(x_1) & \psi_2(x_2) & \dots & \psi_2(x_N) \\ \dots & \dots & \dots & \dots \\ \psi_N(x_1) & \psi_N(x_2) & \dots & \psi_N(x_N) \end{vmatrix} = |\psi_1\psi_2\dots\psi_i\psi_j\dots\psi_n| \quad (1)$$

for which the corresponding energy is given by

$$\begin{aligned} \langle \Psi | \hat{H} | \Psi \rangle &= H_0 + \sum_{i=1}^N \langle \psi_i | \hat{h} | \psi_i \rangle \\ &+ \frac{1}{2} \sum'_{i,j} \{ \langle \psi_i \psi_j | g | \psi_i \psi_j \rangle - \langle \psi_i \psi_j | g | \psi_j \psi_i \rangle \}. \end{aligned} \quad (2)$$

In (2), H_0 represents the nuclear–nuclear repulsion, whereas \hat{h} contains the one-electron kinetic energy operator as well as the operator for the attraction of one electron from all the nuclei. Finally

$$\langle \psi_r \psi_s | g | \psi_p \psi_q \rangle = \iint \psi_r^*(\vec{r}) \psi_s^*(\vec{r}_2) \frac{e^2}{r_{12}} \iint \psi_p(\vec{r}_1) \psi_q(\vec{r}_2) d\mathbf{v}_1 d\mathbf{v}_2 \quad (3)$$

is a two-electron repulsion integral between the charge distributions $\psi_r^*(\vec{r}_1) \psi_p(\vec{r}_1)$ and $\psi_s^*(\vec{r}_1) \psi_q(\vec{r}_1)$. Thus, the third term on the right hand side of (2) constitutes the Hartree term E_H describing the Coulomb interaction of the electron density with itself whereas the last term is the HF-exchange energy E_X^{HF} . In practical calculations, the “occupied orbitals” defining Ψ are written as a linear combination of known atomic orbitals (LCAO) also referred to as basis functions

$$\psi_i = \sum_{r=1}^M C_{ri} \chi_r, \quad i = 1, 2, \dots, n; \quad M \geq n, \quad (4)$$

where $\mathbf{C}_i = \{C_{1i}, C_{2i}, \dots, C_{ri}, C_{si}, \dots, C_{Mi}\}$ is a vector containing all expansion coefficients defining orbital ψ_i . The expansion coefficients are now determined in such a way as to minimize $\langle \Psi | \hat{H} | \Psi \rangle$ under the constraint that the set $\{\psi_i; i = 1, n\}$ be orthonormal. This requirement leads to the well-known Hartree–Fock eigenvalue equation in its Roothan [8] formulation

$$\mathbf{F} \mathbf{C}_i = \varepsilon_i \mathbf{S} \mathbf{C}_i \quad (5)$$

from which \mathbf{C}_i can be determined. In (5),

$$S_{rs} = \int \chi_r^*(\vec{r}_1) \chi_s(\vec{r}_1) d\vec{r}_1, \quad (6)$$

whereas $\mathbf{F} = \mathbf{h} + \mathbf{G}$ with

$$h_{rs} = \int \chi_r^*(\vec{r}_1) \hat{h} \chi_s(\vec{r}_1) d\vec{r}_1 \quad (7)$$

and

$$G_{rs} = \sum_{t,u=1}^M P_{t,u} \{ \langle rs | g | tu \rangle - \langle ru | g | ts \rangle \}, \quad (8)$$

whereas

$$P_{tu} = \sum_{j=1}^n C_{tj}^* C_{uj} \quad (9)$$

In the 1950s, the Roothan equation was too complex and computational demanding to be of practical use due to the occurrence of the many two electron repulsion integrals $\langle rs|g|tu \rangle$. Thus, the number of such integrals increases as M^4 with the number of atomic orbitals M . As a consequence, application of the Roothan equation was in the 1950s and 1960s characterized by a number of approximations.

2.1.1 The Wolfberg Helmholtz Approximation and the Extended Hückel Method

In the first LCAO calculation on MnO_4^- , Wolfberg and Helmholtz [13] suggested as early as 1952 to use empirical data such as ionization potentials for the diagonal elements F_{rr} of (5) since F_{rr} represents the energy of an electron in χ_r in the field of the nuclear skeleton and the remaining valence electrons. For the off-diagonal elements, they introduced what has become known as the Wolfberg and Helmholtz (WH) approximation

$$F_{rs} = kS_{rs}[F_{rr} + F_{ss}]/2, \quad (10)$$

where k is an empirical factor usually taken to be close to one.

R. Hoffmann adopted the same approximation when he introduced the extended Hückel (EH) method in 1963 [14]. The EH scheme gained considerable popularity through Hoffmann's masterful analyses of the bonding in classical transition metal complexes and organometallic compounds [15]. To this date, organometallic chemists are influenced by Hoffmann's powerful orbital interaction approach originally based on the EH scheme [16]. The EH method can provide a qualitative description of the bonding. It is also able to some degree to distinguish between the stability of different conformational isomers as illustrated by J.K. Burdett [17] in his angular overlap approach. R.F. Fenske and his (at that time) student M.B. Hall [18] developed a kindred scheme also based on the WH-approximation. Their method has also been used widely in the 1960s and 1970s to analyze chemical bonding in transition metal compounds with many important contributions from M.B. Hall [19]. It is a common feature of all schemes discussed above that they are computationally expedient thanks to the WH-approximation. At the same time, the WH-approximation is too rough to allow for an accurate determination of bond energies and optimized molecular structures in general.

2.1.2 Approaches Based on Integral Approximations

An alternative approach to the one described above has been to reduce the number of two-electron integrals considered in evaluating G of (8) by assuming that the omitted integrals are small. This procedure was adopted by Pople et al. [20] who introduced complete neglect of differential overlaps (CNDO) in which

$$\langle r_{ASB}|g|t_Cu_D\rangle = \delta_{AC}\delta_{BD}\delta_{rt}\delta_{su}\langle r_{ASB}|g|r_{ASB}\rangle, \quad (11)$$

where A , B , C and D are the centres at which the atomic orbitals $\chi_r, \chi_s, \chi_t, \chi_u$, respectively, are situated. The same authors also proposed intermediate neglect of differential overlap (INDO) where (11) applies if A and B represent different centres, whereas all one-center integrals of the form $\langle r_{ASA}|g|t_Au_A\rangle$ are retained. At the highest level of complexity, Pople et al. proposed neglect of diatomic differential overlap (NDDO) with the approximation

$$\langle r_{ASB}|g|t_Cu_D\rangle = \delta_{AC}\delta_{BD}\langle r_{ASB}|g|t_Au_B\rangle. \quad (12)$$

For compounds containing main group s, p elements all three schemes have been employed and improved considerably leading to the widely used AM1 [21] (Austin model 1), PM3 [22] (Parameterized model number 3) and MNDO [23] (modified neglect of differential overlap) methods that all are extensions or modifications of the NDDO approach. The three schemes are able to predict geometries and energetics of s, p main group compounds quite well. Part of the success stems from the fact that the required one and two centre integrals are parameterized to fit experimental data.

In the case of transition metal complexes, the CNDO theory was first applied by Dahl and Ballhausen [24] to MnO_4^- . Their scheme was later extended to INDO by Ziegler [25] and implemented into the general package ODIN [26]. Better known is the INDO program ZINDO [27] by M. Zerner and the NDDO implementation due to D.S. Marynick [28]. Both have been applied with some success in transition metal chemistry for structure determination and studies of excited states. Attempts have also been made to extend AM1, PM3 and MNDO to transition metals. All in all it must be said that the methods based on integral approximations have been more prolific in studies of main group compounds than transition metal complexes. The reason for that is likely the considerable extra complexity added by the d -orbitals combined with the fact that other attractive schemes are available for d -block compounds.

2.1.3 Ab Initio Hartree Fock with Full Integral Evaluation

The 1960s were barely drawing to an end before I.H. Hillier and V.R. Saunders in Manchester [29] as well as A. Veillard in Strasbourg [30] published the first ab initio Hartree Fock calculations on transition metal complexes without integral approximations. It seemed as if the stage had been set for series of nearly quantitative studies of coordination compounds in the 1970s, without possible errors introduced by an approximate evaluation of \mathbf{F} in (5). However, already a few years into the 1970s it became apparent that the ab initio Hartree Fock results were far from quantitative especially for complexes of $3d$ -elements. Thus, optimized metal–ligand distances were often much too long and calculated

metal–ligand dissociation energies too small as exemplified by early studies on ferrocene [31] and $\text{Cr}(\text{CO})_6$. Also orbital plots based on ab initio Hartree Fock calculations often made less chemical sense than those based on the “approximate” schemes. By the end of the 1970s, the sobering consensus had been reached that ab initio Hartree Fock only is the first step and that more demanding post-HF methods where electron correlation is considered had to be introduced in order to obtain quantitative results. The developments of such schemes will be discussed in Sect. 2.3.

2.2 Density Functional Theory and the Kohn–Sham Equation

In the yearly 1970s, a new electronic structure approach found its way from the physics to the chemistry community in the form of density functional theory (DFT), where the total energy of an electronic system is expressed as a functional of the total electronic density. The basic notion in DFT that the energy of an electronic system can be expressed in terms of its electronic density is almost as old as quantum mechanics and dates back to the early work by P.A.M. Dirac [32], E. Fermi [33] and L.H. Thomas [34].

J.C. Slater [35] embrace in part this idea in 1951 when he replaced the Hartree–Fock exchange energy E_X^{HF} appearing as the last term on the right hand side of (2) with the simple expression

$$E_X^{\text{HFS}} = -9/4\alpha_{\text{ex}}[3/4\pi]^{1/3} \sum_{\gamma} \int [\rho_1^{\gamma}(\vec{r}_1)]^{4/3} d\vec{r}_1 \quad (13)$$

depending only on the density of electrons of either α or β spin. This approximation where α_{ex} is an adjustable parameter evolved out of the need to develop techniques that were able to handle solids within a reasonable time frame. The actual dependence of E_X^{HFS} on $\rho_1^{\gamma}(\vec{r}_1)$ can be justified based on a simple model for exchange [36]. Slater [37] has given a vivid account of how his Hartree–Fock–Slater or $X\alpha$ method evolved during the 1950s and 1960s with reference to numerous applications up to 1974.

The Thomas–Fermi method and the $X\alpha$ scheme were at the time of their inceptions considered as useful models based on the notion that the energy of an electronic system can be expressed in terms of its density. A formal proof of this notion came in 1964 when it was shown by Hohenberg and Kohn [38] that there is a unique relation between density and energy. The year after Kohn and Sham put forward a practical variational DFT approach in which they replaced E_X^{HF} of (2) with a combined exchange and correlation term

$$E_{\text{XC}}^{\text{KS}} = E_X^{\text{KS}} + E_X^{\text{KS}} = \sum_{\gamma}^{\alpha, \beta} \int \rho^{\gamma}(\vec{r}_1) \varepsilon_{\text{XC}}[\rho^{\alpha}(\vec{r}_1), \rho^{\beta}(\vec{r}_1)] d\vec{r}_1, \quad (14)$$

where the energy density ε_{XC} is a functional of $\rho^\alpha(\vec{r}_1), \rho^\beta(\vec{r}_1)$. As in the HF case, the N (Kohn–Sham) orbitals can be expanded into atomic orbitals according to (4). Furthermore, the expansion coefficients C_i can be determined by requiring that they optimize the total (Kohn–Sham) energy. This results in the (Kohn–Sham) matrix equation similar to (5)

$$\mathbf{F}^{\text{KS}} \mathbf{C}_i = \varepsilon_i \mathbf{S} \mathbf{C}_i \quad (15)$$

where now

$$F_{rs}^{\text{KS}} = \int \chi_r(\vec{r}_1) [\hat{h} + V_{\text{C}}(\vec{r}_1) + V_{\text{XC}}(\vec{r}_1)] \chi_s(\vec{r}_1) d\vec{r}_1. \quad (16)$$

Furthermore

$$\begin{aligned} V_{\text{C}}(1) &= \int \frac{\rho(\vec{r}_2)}{|\vec{r}_1 - \vec{r}_2|} d\vec{r}_2 = \sum_i^N \int \frac{\psi_i(\vec{r}_2) \psi_i(\vec{r}_2)}{|\vec{r}_1 - \vec{r}_2|} d\vec{r}_2 \\ &= \sum_{t,u}^M P_{tu} \int \frac{\chi_t(\vec{r}_2) \chi_u(\vec{r}_2)}{|\vec{r}_1 - \vec{r}_2|} d\vec{r}_2, \end{aligned} \quad (17)$$

where the exchange correlation potential V_{XC} is given as the functional derivative of the exchange correlation energy with respect to the density or

$$V_{\text{XC}} = \partial E_{\text{XC}} / \partial \rho. \quad (18)$$

2.2.1 Practical Implementations of the Kohn–Sham Method

In the earliest implementation applied to molecular problems, K. Johnson [39] used scattered-plane waves as a basis and the exchange-correlation energy was represented by (13). This SW- $X\alpha$ method employed in addition an (muffin-tin) approximation to the Coulomb potential of (17) in which V_{C} is replaced by a sum of spherical potentials around each atom. This approximation is well suited for solids for which the SW- $X\alpha$ method originally was developed [40]. However, it is less appropriate in molecules where the potential around each atom might be far from spherical. The SW- $X\alpha$ method is computationally expedient compared to standard ab initio techniques and has been used with considerable success [41] to elucidate the electronic structure in complexes and clusters of transition metals. However, the use of the muffin-tin approximation precludes accurate calculations of total energies. The method has for this reason not been successful in studies involving molecular structures and bond energies [42].

The first implementations of a self-consistent KS-scheme, without recourse to the muffin-tin approximations, are due to Ellis and Painter [43], Baerends et al. [44], Sambe and Felton [45], Dunlap et al. [46] as well as Gunnarson et al. [47]. The accurate representation of V_C is in general accomplished by fitting the molecular density to a set of one-center auxiliary functions [44, 46] $f_\eta(\vec{r}_1)$ as

$$\rho(\vec{r}_1) \approx \sum_{\eta} a_{\eta} f_{\eta}(\vec{r}_1) \quad (19)$$

from which the Coulomb potential can be calculated analytically [44, 46] in each point \vec{r}_1 as

$$V_C(\vec{r}_1) = \sum_{\eta} \int \frac{a_{\eta} f_{\eta}(\vec{r}_2)}{|\vec{r}_1 - \vec{r}_2|} d\vec{r}_2. \quad (20)$$

The matrix elements F_{rs}^{KS} can subsequently be obtained from numerical integration as

$$F_{rs}^{\text{KS}} = \sum_k [\chi_r(\vec{r}_k) \hat{h} \chi_s(\vec{r}_k) + \chi_r(\vec{r}_k) V_C(\vec{r}_k) \chi_s(\vec{r}_k) + \chi_r(\vec{r}_k) V_{\text{XC}}(\vec{r}_k) \chi_s(\vec{r}_k)] W(\vec{r}_k), \quad (21)$$

where $W(\vec{r}_k)$ is a weight factor [43, 48–52]. F_{rs}^{KS} can now be evaluated as $\chi_r(\vec{r}_k)$, $\chi_s(\vec{r}_k)$, $\hat{h} \chi_r(\vec{r}_k)$, $V_C(\vec{r}_k)$, $V_{\text{XC}}(\vec{r}_k)$ and $W(\vec{r}_k)$ readily are calculated at each sample point \vec{r}_k . The extensive use of numerical integration [43, 48–52] is amiable to modern vector machines. Numerical integration also makes it easy to deal with complicated expressions for V_{XC} . The often intricate form of V_{XC} and $E_{\text{XC}}^{\text{KS}}$ precludes on the other hand a completely analytical evaluation of F_{rs}^{KS} and E^{KS} .

Some of the earliest DFT programs such as ADF [44] and DMOL [50] make use of Slater-type orbitals (STOs), which necessitated that all parts of F_{rs}^{KS} and E^{KS} are calculated by numerical integration. In that case, special care must be exercised in order to calculate total energies [53, 54], energy gradients [55] and energy Hessians [56–58] sufficiently accurate. Other early packages including LCGTO [45, 46], DeMon [59], DGauss [60] and ParaGauss [61]. Later adaptations have also been introduced into Gaussian, QChem, Jaguar, Spartan, Turbomol, Dalton, Gamess BDF [62], Molpro, Molcas ORCA, all make use of Gaussian-type orbitals (GTOs) where only the exchange-correlation part of F_{rs}^{KS} and E^{KS} is evaluated by numerical integration. However in several of these packages fitting of the density as in (19) is employed to speed up the calculation of Coulomb integrals by making use of the resolution of the identity [63, 64] or Cholesky decomposition techniques [65, 66]. A unique approach has been taken by A. Becke in which the Kohn–Sham orbitals and energy are optimized without the use of basis functions as in (4). The approach implemented in the Numol program [67] was first applied to diatomic molecules and later also to polyatomic systems.

2.2.2 The Development of New Density Functionals

The quality of the DFT calculations obviously depends on how well the approximate expression for E_{XC}^{KS} represents the exact (but unknown) exchange correlation functional. Throughout the 1970s, the large majority of DFT calculations were based on the local density approximation (LDA) in which the exchange E_X^{LDA} [68] and correlation E_C^{LDA} [69] energies both are taken from the homogeneous electron gas and expressed as a simple function of the electron density with E_X^{LDA} quite similar to E_X^{HFS} of (13) where $\alpha_{ex} = 2/3$. The LDA calculations afforded in general metal–ligand distances in much better agreement with experiment than HF as shown in Table 1. Furthermore, orbital plots based on LDA tended to make more chemical sense than those from HF calculations.

It might seem surprising that the “approximation” of E_X^{HF} by E_X^{LDA} should lead to substantially better structures. An extensive analysis [74, 75] has shown that the difference $E_X^{LDA} - E_X^{HF}$ which is added to E_X^{HF} in order to obtain E_X^{LDA} in fact to some degree mimic “static correlation” which is absent in the HF-scheme. Unfortunately, towards the end of the 1970s when the DFT-based methods finally were sufficiently numerically stable [53, 54] to calculate metal–ligand dissociation energies, it became evident that the LDA scheme systematically overestimates bond energies. Thus after one decade of excitement, it seemed as if practical DFT calculations would be limited in scope and unable to deal with the subject of reactivity and thermochemistry.

This prospect was changed when A. D. Becke through a series of seminal papers [76–78] introduced expressions for E_{XC}^{KS} that depended not only on the density ρ but also on its gradient $\nabla\rho$. This modification has become known as the generalized gradient approximation (GGA) and it significantly improved the accuracy of the energetics as shown in Table 2. Well-known GGAs are BP86 and BLYP in which the exchange part is due to Becke [76] and the correlation based on the work of Perdew [80] and Lee [81] et al., respectively.

The work by Becke had a profound impact on the quantum chemistry community. Thus by 1992 most theoretical chemists that up to that time had been sceptical about DFT embraced the method and in a short period DFT was incorporated into

Table 1 A comparison of bond distances (Å) from HF and LDA calculations with experiment

	A–B	HF	LDA	Expt
Fe(CO) ₅	Fe–C _{ax}	2.047 ^a	1.774 ^b	1.807
	Fe–C _{eq}	1.874 ^a	1.798 ^b	1.827
Fe(C ₅ H ₅) ₂	Fe–C	1.88 ^c	1.60 ^d	1.65
HCo(CO) ₄	Co–C _{eq}	2.02 ^e	1.753 ^f	1.764
	Co–C _{ax}	1.96 ^e	1.779 ^f	1.818

^a[68]

^b[70]

^c[69]

^d[71]

^e[72]

^f[73]

Table 2 First metal-carbonyl dissociation energy (kJ/Mol) in a number of metal carbonyls^a

Molecule	HFS	LDA	BP86	Exp
Cr(CO) ₆	278	276	147	162
Mo(CO) ₆	226	226	119	126
W(CO) ₆	247	249	142	166
Ni(CO) ₄	194	192	106	104

^a[79]**Table 3** Calculated metal-ligand bond length^a

Compound	Bond	B3LYP	Exp
TiF ₄	Ti–F	1.74	1.75
TiCl ₄	Ti–Cl	2.17	2.17
Cr(CO) ₆	Cr–C	1.91	1.92
Cr(C ₆ H ₆)(CO) ₃	Cr–C (C ₆ H ₆)	2.23	2.21
Cr(C ₆ H ₆)(CO) ₃	Cr–C (CO)	1.85	1.86
Mn ₂ (CO) ₁₀	Mn–Mn	2.96	2.98
Mn ₂ (CO) ₁₀	Mn–C _{ax}	1.80	1.80
Mn ₂ (CO) ₁₀	Mn–C _{eq}	1.85	1.87
Fe(CO) ₅	Fe–C _{ax}	1.81	1.81
Fe(CO) ₅	Fe–C _{eq}	1.80	1.83
Fe(C ₅ H ₅) ₂	Fe–C	2.06	2.06
Fe(C ₂ H ₄)(CO) ₄	Fe–C(CO)	2.11	2.12
Fe(C ₂ H ₄)(CO) ₄	Fe–C _{ax}	1.81	1.82
Fe(C ₂ H ₄)(CO) ₄	Fe–C _{eq}	1.79	1.81
CoH(CO) ₄	Co–C _{eq}	1.79	1.82
Co ₂ (CO) ₄	Co–Co	2.61	2.53
Ni(CO) ₄	Ni–C	1.81	1.84
CuF	Cu–F	1.66	1.75
Mean absolute error		0.02	

^aFrom [88]. Distances in Å

all major program packages such as Gaussian, Gamess and Turbomol. The popularity of DFT has led to the development of many new functionals as reviewed elsewhere [82–87].

Perhaps the most popular has been the hybride functional B3LYP [78] by Becke in which 20% of E_X^{LYP} is replaced by E_X^{KS} . We present in Table 3 a number of metal–ligand distances optimized by B3LYP [88]. For most systems, the error is only 0.02 Å. In Table 4, we compare metal–ligand bond energies calculated by BLYP [76, 81] and B3LYP [76, 80]. Obviously, B3LYP represents a clear improvement over BLYP.

Progress in the development of functionals have up to now involved modeling of both E_X^{KS} and E_C^{KS} . However, some theoreticians including Becke are increasingly of the opinion that further progress in DFT will require the use of exact exchange E_X^{HF} for E_X^{KS} . What is left is to augment the approximate E_C^{KS} functionals which only consider dynamic correlation with static correlation. Becke has introduced such functionals DF07 [89] in which static correlation is modeled by modified

Table 4 Average M-L dissociation energies^a

Complex	BLYP	B3LYP	DF07 ^b	Exp
Cr(CO) ₅	29.7	22.8	25.0	23.4
Cr(CO) ₆	30.6	24.8	26.9	25.6
Mn ₂ (CO) ₁₀	28.6	20.3	22.9	22.7
MnH(CO) ₅	34.7	27.4	29.0	27.4
Fe(CO) ₄	33.7	23.4	25.8	24.7
Fe(CO) ₅	34.0	25.9	28.4	28.0
Co ₂ (CO) ₈	40.4	26.4	31.2	30.6
CoH(CO) ₄	45.6	36.9	38.1	36.9
Ni(CO) ₃	36.5	35.0	39.1	38.8
Ni(CO) ₄	41.7	32.5	34.5	35.3

^aFrom [88] with energy in kcal/mol^bFunctional due to Becke from [89]

expressions for $E_X^{\text{LDA}} - E_X^{\text{HF}}$. It can be seen in Table 3 that the results [88] are quite encouraging. For a larger sample of systems, the mean absolute error was 6.3 kcal/mol, 4.3 kcal/mol and 2.3 kcal/mol for BLYP, B3LYP and DF07 [89], respectively. It is in a way ironic that DFT from its promising $X\alpha$ start with a local exchange approximation $E_X^{\text{X}\alpha}$ is back to Hartree–Fock and E_X^{HF} as a starting point.

2.3 Post-Hartree–Fock Methods

It is an attractive feature of ab initio wave function theory that there is a clear hierarchy of methods leading from Hartree–Fock to the exact solution of the Schrödinger equation. Post-Hartree–Fock methods can be divided into three main categories [88]. The first is based on (Møller–Plesset) perturbation theory [89] and referred to as *MPn* where *n* is the order of the perturbation. *MPn* is excellent when Hartree–Fock already is giving a reasonable description, as is often the case for complexes involving 4*d* and 5*d* elements. Otherwise, it fails or might only converge slowly with the order *n*. *MP2* can be used for medium size systems of 100–200 atoms.

The second category is based on configuration interaction (CI) in which the HF determinant Ψ_0 is augmented by a number of determinants Ψ_k constructed from Ψ_0 by replacing one or more of the occupied HF orbitals with virtual HF orbitals

$$\Psi_{\text{CI}} = \sum_{k=0}^n D_k \Psi_k. \quad (22)$$

In simple CI, the expansion coefficients D_k are optimized in such a way that Ψ_{CI} has the minimum energy. The expansion in (22) can be slowly converging requiring millions of terms. The number of needed terms can be reduced in the multi-configuration SCF procedure (MCSCF), where both D_k and the orbital expansion

coefficients of (4) are optimized simultaneously with respect to the energy of Ψ_{CI} [88]. One of the better known MCSCF schemes is the complete active space self-consistent field method (CASSCF) [90]. In this scheme, one considers an active space of M_{occ} occupied HF orbitals and M_{vir} virtual HF orbitals. From this space, Ψ_{CI} is constructed by taking into account all possible displacement of orbitals from M_{occ} to M_{vir} . As the number of terms in (22) rapidly goes up with the size of the active space, a more limited number of terms can be selected in the restricted active space self-consistent field method (RASSCF). Both CASSCF and RASSCF can be augmented with second-order perturbation theory in CASPT2 and RASPT2 [91]. CASSCF, RASSCF as well as CASPT2, RASPT2 have been used extensively in transition metal chemistry. They are the methods of choice in those cases where a system is poorly described by a single Slater determinant. Other methods that can be used in a similar situation are the generalized valence bond method (GVB) [92], valence bond theory (VB) [93] and the symmetry adapted cluster/configuration interaction (SAC-CI) method [94]. All of these methods scale as $(n_e)^5$ or worse with the number of electrons n_e and can as a consequence only be used for smaller systems.

The third and last category is the couple cluster (CC) method [88]. In this scheme, one writes the wave function Ψ_{CC} as

$$\Psi_{\text{CC}} = e^T \Psi_0, \quad (23)$$

with

$$e^T = 1 + T + \frac{1}{2}T^2 + \frac{1}{6}T^3 + \sum_{k=0}^{\infty} \frac{1}{k!}T^k \quad (24)$$

and the cluster operator T given by

$$T = T_1 + T_2 + T_3 + \dots T_N + \dots \quad (25)$$

Here, the T_i operator when working on Ψ_0 affords the i th excited Slater determinants. In practical, CC calculations T of (25) is truncated. Thus keeping $T_1 + T_2$ gives rise to CCSD whereas the addition of T_3 and subsequently T_4 leads to CCSDT and CCSDTQ, respectively. The CCSD scheme which scales as $(n_e)^6$ is used routinely for up to 100 electrons. It is considered as the most accurate method for metal complexes in those cases where the reference HF determinant Ψ_0 affords a reasonable description. CCSDT and CCSDTQ scales as $(n_e)^8$ and $(n_e)^{10}$, respectively, they can only be used for very small systems.

2.4 Applications to the Ground State of Permanganate and Related Tetroxo Systems

The methods described above have been applied to ground state properties of a large number of complexes. These properties include parameters from infrared

(IR), Raman nuclear magnetic resonance (NMR), electron spin resonance (ESR), Mössbauer and vibronic circular (VCD) spectroscopy as well as electric and magnetic dipole moments, polarizability and magnetic susceptibility [83]. We shall in the following as an example discuss some applications to permanganate and related tetroxo complexes.

2.4.1 Electronic Structure of Permanganate

The permanganate anion MnO_4^- has a tetrahedral geometry with a T_d point group symmetry, Fig. 1. At each oxygen atom, we have a core like $2s$ orbital as well as two $2p_\pi$ and one $2p_\sigma$ valence orbitals. The total number of valence electrons is 32 of which 8 are in core type $2s$ levels and the remaining 24 in molecular orbitals spanned by $2p_\pi$, $2p_\sigma$ and $3d$. We show in Fig. 2 the levels represented by orbitals made up of $2p_\pi$, $2p_\sigma$ and $3d$.

The lowest level is represented by $1t_2$ which is a bonding combination between a d orbital transforming as t_2 and a t_2 ligand combination. The corresponding anti-bonding combination is given by the empty $3t_2$ orbital, Fig. 3. Slightly above is the $1e$ level corresponding to the bonding combination between a d orbital transforming as e and a ligand combination of e -symmetry. The related anti-bonding combination is $2e$, Fig. 3. Further above is $1a$ made up of $2p_\sigma$ ligand combinations interacting in-phase with $4s$ on the metal. At highest energy among the occupied orbitals are the $2t_2$ and $1t_1$ combinations that both are ligand based with no contributions from the metal, Table 3. The empty $3t_2$ and $2e$ levels correspond to the d many- fold split by the ligand orbitals with $2e$ below $3t_2$ as predicted by ligand field theory [5]. The compositions and relative energies of the frontier orbitals for MnO_4^- is what one would obtain from an LDA or GGA calculation [36] on MnO_4^- . It is interesting to note that Wolfberg and Helmholtz [13] in the very first LCAO calculation on MnO_4^- found $2e$ above $3t_2$ in

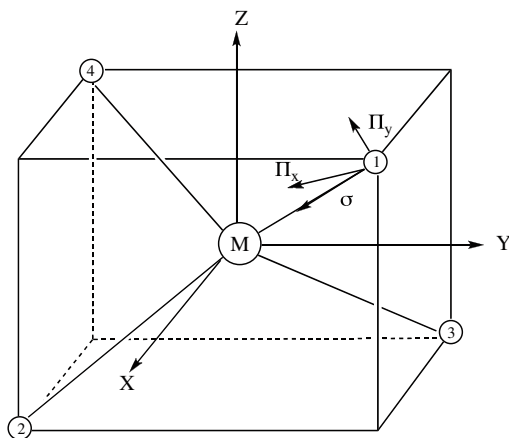


Fig. 1 Geometry of MnO_4^-

Fig. 2 Orbital level diagram for MnO_4^-

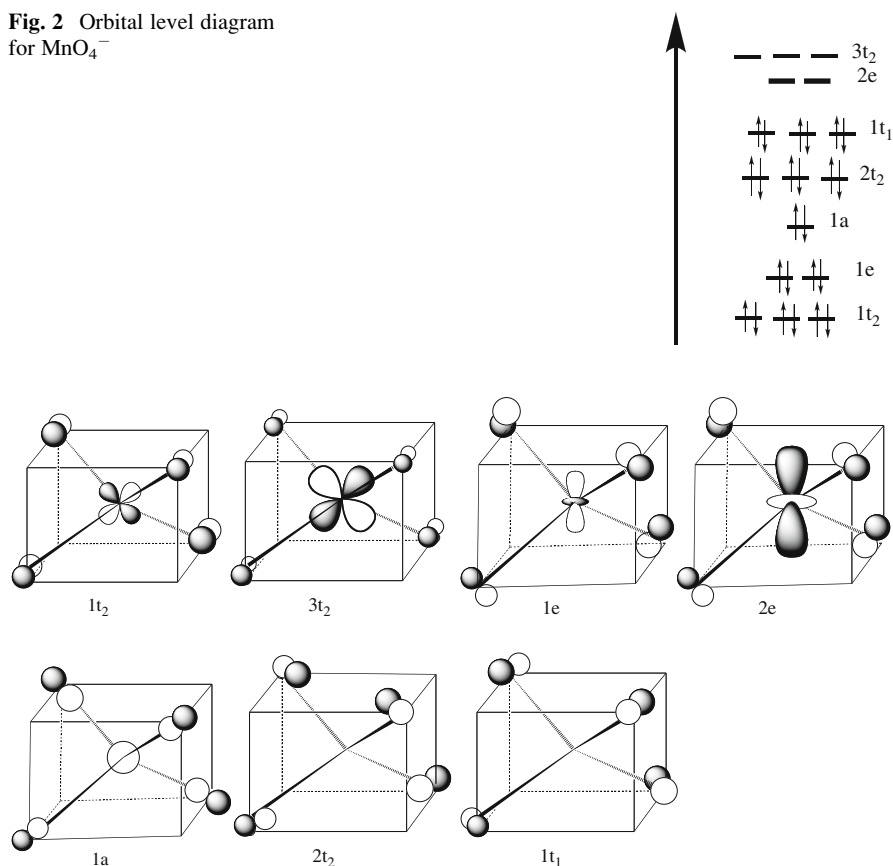


Fig. 3 Frontier molecular orbitals of MnO_4^-

disagreement with ligand field theory. Later calculations both based on wave function theory and DFT have always recovered the ligand field ordering.

There has been a number of HF ab initio calculations on MnO_4^- [95–102]. All of these calculations exhibit a very different picture from that of Fig. 3 with $1t_2$ being a pure d -orbital and $1e$ exclusively a ligand orbital. Thus, HF reveals an ionic bonding mode as opposed to the covalent DFT picture displayed in Fig. 3. Buijse and Baerends have analyzed the bonding in MnO_4^- based on HF, post-HF and DFT calculations [103]. They point out the special circumstances encountered in complexes of $3d$ elements where one has $3s$ and $3p$ core-type orbitals of the same radial extent as $3d$. The $3s, 3p$ orbitals will interact repulsively with the ligands making it impossible to reach metal–ligand distances where the $3d$ to ligand overlaps are optimal. The HF method responds to the relatively weak metal–ligand interactions by localizing the electrons on either the metal or the ligands in each orbital and thus optimize the exchange interaction. The covalent bond picture provided by DFT is recovered nicely in extensive CI and MCSCF calculations.

At the HF-level, MnO_4^- is unstable with respect to dissociation into one electron and the neutral species. Introducing post-HF calculations makes MnO_4^- stable with respect to such a dissociation. The problems encountered for HF in $3d$ metal complexes are not present in systems involving nd ($n = 4,5$) elements since the corresponding ns , np orbitals are much more contracted than nd for $n = 4,5$. Also, the HF error seems to be more severe for late $3d$ elements than early $3d$ elements.

2.4.2 ^{17}O Chemical Shifts in Permanganate and Related Tetroxo Systems

There are a number of spectroscopic parameters that can be formulated as the second derivative of the total energy with respect to two perturbations [88]. One such parameter is the nuclear shielding tensor [104]

$$\sigma_{st}^N = \left(\frac{\delta^2 E}{\delta B_s \delta \mu_t^N} \right)_{(\vec{B}=0, \vec{\mu}^N=0)}, \quad (26)$$

where B_r , μ_t^N are Cartesian components of, respectively, an external homogeneous magnetic field \vec{B} and a nuclear magnetic moment $\vec{\mu}^N$ of nucleus N. Related to the shielding tensor of nuclei N is the shielding constant

$$\sigma^N = \frac{1}{3} [\sigma_{xx}^N + \sigma_{yy}^N + \sigma_{zz}^N] \quad (27)$$

as well as the chemical shift given by

$$\delta^N = \sigma^N - \sigma^{\text{ref}}. \quad (28)$$

Here, σ^{ref} is the shielding constant of the reference with respect to which the chemical shift δ^N of nuclei N is measured. Finally, the shielding tensor component σ_{st}^N has a diamagnetic contribution $\sigma_{st}^{d,N}$ and a paramagnetic contribution $\sigma_{st}^{p,N}$. Here $\sigma_{st}^{d,N}$ only depends on the occupied ground state orbitals whereas $\sigma_{st}^{p,N}$ depends on the coupling between ground state occupied and virtual orbitals induced by the external homogeneous magnetic field \vec{B} [104]. We present in Table 5 the ^{17}O chemical shift of several tetroxo complexes including permanganate.

It is clear from Table 5 that the chemical shifts calculated with HF are too negative with the possible exception of the two $5d$ complexes WO_4^{2-} and ReO_4^- . The agreement with experiment is especially poor for MnO_4^- . An analysis reveals that the deviation for permanganate comes from the paramagnetic contribution $\sigma_{st}^{p,N}$, where the coupling between occupied and virtual orbitals are exaggerated due to their localized nature. Thus, occupied and virtual orbitals both localized on either the metal or the ligands will lead to a strong coupling. Introducing next the MP2 method is seen to lead to an overcompensation, where most shifts goes from negative in HF to positive in MP2. On the other hand, the GGA scheme BP86

Table 5 ^{17}O Chemical shifts [ppm] for tetroxo complexes calculated by different methods and compared to experiment

Compound	HF ^a	MP2 ^a	BP86 ^b	B3LYP ^a	Exp ^a
WO_4^{2-}	−194	−21	−140	−183	−129
MoO_4^{2-}	−335	−60	−251	−289	−239
CrO_4^{2-}	−1,308	2,173	−508	−640	−544
ReO_4^-	−464	3	−282	−339	−278
TcO_4^-	−819	184	−421	−518	−458
MnO_4^-	−7,248	54,485	−832	−1,149	−939
OsO_4	−1,295	1,069	−517	−657	−505
RuO_4	−3,330	8,262	−740	−1,037	−820

^a[105]^b[106]

with delocalized orbitals, Fig. 3, and a covalent bonding description leads to shifts in reasonable agreement with experiment for all systems, even permanganate. Adding 20% HF exchange in the hybrid B3LYP leads as expected to more negative shifts but not to an overall improved agreement with experiment.

2.4.3 M-O Spin–Spin Coupling Constants in Permanganate and Related Tetroxo Systems

Another spectroscopic parameter that we can write as a second-order energy derivative is the spin–spin coupling tensor of NMR defined as [107–109]

$$K_{st}^{\text{AB}} = \left(\frac{\delta^2 E}{\delta \mu_s^{\text{A}} \delta \mu_t^{\text{B}}} \right)_{(\vec{\mu}^{\text{A}}=0, \vec{\mu}^{\text{B}}=0)}, \quad (29)$$

where $\mu_s^{\text{A}}, \mu_t^{\text{B}}$ are Cartesian components of the nuclear magnetic moments $\vec{\mu}^{\text{A}}$ and μ_t^{B} on nuclei A and B, respectively. Related to the coupling tensor K_{st} is the reduced coupling constant

$$K_{\text{AB}} = \frac{1}{3} [K_{xx}^{\text{AB}} + K_{yy}^{\text{AB}} + K_{zz}^{\text{AB}}]. \quad (30)$$

There are four contributions to K_{AB}

$$K_{\text{AB}} = K_{\text{AB}}^{\text{FC}} + K_{\text{AB}}^{\text{PSO}} + K_{\text{AB}}^{\text{DSO}} + K_{\text{AB}}^{\text{SD}}, \quad (31)$$

represented by the Fermi-contact term ($K_{\text{AB}}^{\text{FC}}$), the paramagnetic spin-orbit term ($K_{\text{AB}}^{\text{PSO}}$), the diamagnetic spin-orbit term ($K_{\text{AB}}^{\text{DSO}}$) and the spin-dipolar term ($K_{\text{AB}}^{\text{SD}}$). Of these the first two are in most cases dominating.

We compare in Table 6 calculated [107] reduced coupling constants K_{MO} based on BP86 with experiment. The agreement is in general good with the possible exception of MnO_4^- . The largest contribution comes from the Fermi-contact term

Table 6 Reduced coupling constants ^{a,b} K_{MO} in some tetroxo complexes

Molecule	$R_{\text{M-O}}$	^c $K_{\text{MO}}^{\text{FC}}$	^d $K_{\text{MO}}^{\text{PSO}}$	^e K_{MO} calculated	K_{MO} Exp
VO_4^{3-}	1.711	243	-94	150	144
CrO_4^{2-}	1.653	244	-140	104	108
MnO_4^-	1.629	218	-189	29	75
MoO_4^{2-}	1.765	464	-118	346	380
TcO_4^-	1.676	531	-128	403	359

^aIn SI units of $10^{19} \text{ kg m}^{-2} \text{ s}^{-2} \text{ A}^{-2}$ ^bFrom [107]^cFermi-contact contribution^dParamagnetic spin-orbit contribution^eTotal reduced coupling constant

$K_{\text{MO}}^{\text{FC}}$, Table 6. This term arises from a generation of net spin-density at the position of the metal nuclei due to the nuclear magnetic moments on the oxygen $\bar{\mu}^{\text{O}}$. The generation of net spin density requires the coupling of occupied and virtual ground state orbitals of a_1 symmetry with contributions from both $2s$ orbitals on oxygen and $3s, 4s$ orbitals on the metal. $K_{\text{MO}}^{\text{FC}}$ is as explained elsewhere [107] positive for all the systems and larger for complexes of $4d$ -elements than $3d$ -elements. The second important contribution is $K_{\text{MO}}^{\text{PSO}}$. It arises when the magnetic field due to the magnetic dipole of the metal couples occupied and virtual orbitals to generate a current density that interacts with the nuclear magnetic moment of the oxygens. The negative $K_{\text{MO}}^{\text{PSO}}$ is established by the coupling between $1t_2$ and $3t_2$. It is proportional to the coupling integral between the two orbitals as well as $1/(\varepsilon_{3t_2} - \varepsilon_{1t_2})$. As MnO_4^- has the smallest $\varepsilon_{3t_2} - \varepsilon_{1t_2}$ energy gap, it has the most negative contribution from $K_{\text{MnO}}^{\text{PSO}}$ and the smallest K_{MnO} . In fact, it is likely that $K_{\text{MnO}}^{\text{PSO}}$ is too negative for MnO_4^- , leading to a too small estimate of K_{MnO} .

3 Excited State Electronic Structure Theory

The development of electronic structure theories for metal complexes has always been closely linked with electron spectroscopy of transition metal compounds. We shall in the following describe both DFT and wave function methods that have been used in the study of excited states. We shall also discuss their application to the tetroxo systems.

3.1 Different DFT-Based Methods Used in the Study of Excited States

As we have seen in Sect. 2, KS-DFT has been very successful in dealing with ground state properties, especially for closed shell molecules. KS-DFT owes this

success to its simplicity as well as the development of increasingly accurate energy density functionals $\varepsilon[\rho]$ or exchange correlation potentials $V_{\text{XC}}[\rho]$ [82–87]. There has been considerable interest in also applying KS-DFT to excited states.

3.1.1 Variational DFT Approaches in the Study of Excited States

The first category of DFT-based methods applied to excited states is the variational approaches. They include ensemble DFT [110, 111], variation of bifunctionals [112] and Δ DFT/ Δ SCF-DFT [36, 113–116]. Of the variational methods, Δ DFT/ Δ SCF-DFT can be readily implemented and applied whereas only few applications have appeared based on the two first approaches due to their computational complexity. In Δ DFT/ Δ SCF-DFT [36, 113–116], one generates new “excited state” KS-Slater determinants from the ground state determinant by substituting one (or more) of the occupied ground state KS-orbitals with one or more ground state virtual KS-orbitals. An evaluation of the energy of the new determinants followed by subtraction of the ground state energy makes it possible to determine excitation energies corresponding to one-, two- and multi-electron excitations. In addition, the Δ SCF-DFT scheme (but not Δ DFT) allows for the occupied orbitals in the excited state to be optimized variationally.

The Δ DFT/ Δ SCF-DFT scheme has been met with considerable reservation. Thus, Δ DFT/ Δ SCF-DFT assumes implicitly that a transition can be represented by an excitation involving only two orbitals, an assumption that seems not generally to be satisfied. Also, the variational optimization in Δ SCF-DFT of the orbitals makes it difficult to ensure orthogonality between different excited state determinants when many transitions are considered, resulting ultimately in a variational collapse. Finally, it has been questioned [110] whether there exists a variational principle for excited states in DFT. In spite of this, some of the first pioneering chemical applications of DFT involved Δ SCF-DFT calculations on excitation energies [36, 113–116] for transition metal complexes and Δ SCF-DFT is still widely used [117–121].

3.1.2 DFT Approaches in the Study of Excited States Based on Response Theory

A popular alternative to variational approaches in the study of excited state properties is time-dependent DFT (TD-DFT) in its adiabatic formulation [122–128]. In this scheme, one considers the first-order change in the ground state density $\rho^{(\gamma)}(\omega, \vec{r})$ due to a perturbation from the γ -component $E_\gamma(\omega)$ of a frequency-dependent electric field and the associated frequency-dependent polarizability $\alpha^{(\gamma\beta)}(\omega)$. The excitation energies ω_0 are subsequently found as poles or resonances for $\alpha^{(\gamma\beta)}(\omega)$.

The adiabatic TD-DFT approach [122–124] seems to be free of much of the problems associated with Δ SCF-DFT. In the first place, TD-DFT transition energies

ω_0 are calculated from a ground state property $\alpha^{i\beta}(\omega)$ by a frequency-dependent response method rather than excited state variation theory. Furthermore, orthogonality is ensured as all excitation energies are found as eigenvalues to a common matrix constructed from the ground state Hessian [88, 122–124, 129–131].

Extensive benchmarking of adiabatic TD-DFT [132–137] has revealed that the calculated excitation energies are in fair agreement with experiment. It is thus to be expected that adiabatic TD-DFT be used increasingly as a reasonable compromise between accuracy and computational cost in many applications [132–137]. However, the extensive benchmarking has revealed some systematic errors [132–137] in the calculated excitation energies when use is made of the GGA as well as the popular approximate hybrid functionals containing fractions of exact Hartree–Fock exchange. The largest deviations [132–137] are found for transitions where electrons are moved between two separated regions of space (charge transfer transitions) or between orbitals of different spatial extend (Rydberg transitions) [138–140].

Ziegler et al. have in two recent studies [141, 142] analyzed the reason for the deviations between experimental charge transfer (CT) excitation energies and estimates obtained from TD-DFT applications. It was found that the deviations for a large part can be traced back to the simple approach taken in standard TD-DFT where terms depending on the linear orbital response parameter set U only is kept to second order in U for the energy expression [141, 142]. While this simple linear response approach is adequate for the corresponding Hartree–Fock time-dependent formulation where self-interaction is absent [143], it is inadequate for TD-DFT applied to most approximate functionals where self-interaction terms are present [141–143]. In those cases, higher order terms in U must be included into the energy expression [141–143].

With the intention of including higher order terms, we have developed a constricted variational density functional approach (CV(n)-DFT) for the calculation of excitation energies and excited state properties [144, 145]. We shall introduce this method in the next section and show that adiabatic TD-DFT and Δ SCF-DFT both are special cases of the more general constricted variational DFT scheme.

3.1.3 Constricted Variational Density Functional Theory

In the constricted variational density functional theory, CV(n)-DFT, we carry out a unitary transformation [145] among occupied $\{\phi_i; i = 1, \text{occ}\}$ and virtual $\{\phi_a; a = 1, \text{vir}\}$ ground state orbitals

$$Y \begin{pmatrix} \phi_{\text{occ}} \\ \phi_{\text{vir}} \end{pmatrix} = e^U \begin{pmatrix} \phi_{\text{occ}} \\ \phi_{\text{vir}} \end{pmatrix} = \left(\sum_{n=0}^{\infty} \frac{(U^2)^n}{2n!} \right) \begin{pmatrix} \phi_{\text{occ}} \\ \phi_{\text{vir}} \end{pmatrix} = \begin{pmatrix} \phi'_{\text{occ}} \\ \phi'_{\text{vir}} \end{pmatrix}. \quad (32)$$

Here, ϕ_{occ} and ϕ_{vir} are concatenated column vectors containing the sets $\{\phi_i; i = 1, \text{occ}\}$ and $\{\phi_a; a = 1, \text{vir}\}$ whereas ϕ'_{occ} and ϕ'_{vir} are concatenated column vectors containing the resulting sets $\{\phi'_i; i = 1, \text{occ}\}$ and $\{\phi'_a; a = 1, \text{vir}\}$ of

occupied and virtual excited state orbitals, respectively. The unitary transformation matrix Y is in (33) expressed in terms of a skew symmetric matrix U as

$$Y = e^U = I + U + \frac{U^2}{2} + \cdots = \sum_{n=0}^{\infty} \frac{U^n}{n!} = \sum_{n=0}^{\infty} \frac{(U^2)^n}{2n!} + U \sum_{n=0}^{\infty} \frac{(U^2)^n}{(2n+1)!}. \quad (33)$$

Here, $U_{ij} = U_{ab} = 0$ where “ i,j ” refer to the occupied set $\{\phi_i; i = 1, \text{occ}\}$ whereas “ a,b ” refer to $\{\phi_a; a = 1, \text{vir}\}$. Furthermore, U_{ai} are the variational mixing matrix elements that combines virtual and occupied ground state orbitals in the excited state with $U_{ai} = -U_{ia}$. Thus, the entire matrix U is made up of $\text{occ} \times \text{vir}$ independent elements U_{ai} that also can be organized in the column vector \vec{U} . For a given \vec{U} , we can by the help of (33) generate a set of “occupied” excited state orbitals

$$\phi_i' = \sum_p^{\text{occ+vir}} Y_{pi} \phi_p = \sum_j^{\text{occ}} Y_{ji} \phi_j + \sum_a^{\text{vir}} Y_{ai} \phi_a \quad (34)$$

that are orthonormal to any order in U_{ai} .

In the simple CV(2)-DFT theory [144], the unitary transformation of (33) is carried out to second order in U . We thus obtain the occupied excited state orbitals to second order as

$$\phi_i' = \phi_i + \sum_a^{\text{vir}} U_{ai} \phi_a - \frac{1}{2} \sum_j^{\text{occ}} \sum_a^{\text{vir}} U_{ai} U_{aj} \phi_j, \quad (35)$$

from which we can generate the excited state Kohn–Sham density matrix to second order as

$$\begin{aligned} \rho'(1, 1') &= \rho^{(0)}(1, 1') + \Delta\rho'(1, 1') \\ &= \rho^{(0)}(1, 1') + \sum_i^{\text{occ}} \sum_a^{\text{vir}} U_{ai} \phi_a(1') \phi_i^*(1) + \sum_i^{\text{occ}} \sum_a^{\text{vir}} U_{ai}^* \phi_a^*(1) \phi_i(1') \\ &\quad + \sum_i^{\text{occ}} \sum_a^{\text{vir}} \sum_b^{\text{vir}} U_{ai}^* U_{bi} \phi_a(1') \phi_b^*(1) - \sum_i^{\text{occ}} \sum_j^{\text{occ}} \sum_a^{\text{vir}} U_{ai} U_{aj}^* \phi_i(1') \phi_j^*(1). \end{aligned} \quad (36)$$

The expression for $\rho'(1, 1')$ makes it next possible to write down the corresponding excited state Kohn–Sham energy to second order as

$$\begin{aligned} E_{KS}[\rho'(1, 1')] &= E_{KS}[\rho^0] + \sum_{ai} U_{ai} U_{ai}^* (\epsilon_a^0 - \epsilon_i^0) + \sum_{ai} \sum_{bj} U_{ai} U_{bj}^* K_{ai,bj} + \frac{1}{2} \\ &\quad \times \sum_{ai} \sum_{bj} U_{ai} U_{bj} K_{ai,jb} + \frac{1}{2} \sum_{ai} \sum_{bj} U_{ai}^* U_{bj}^* K_{ai,jb} + O[U^{(3)}]. \end{aligned} \quad (37)$$

Here, $E_{\text{KS}}[\rho^0]$ is the ground state energy and “ a, b ” run over virtual ground state canonical orbitals, whereas “ i, j ” run over occupied ground state canonical orbitals. Furthermore

$$K_{ru,tq} = K_{ru,tq}^{\text{C}} + K_{ru,tq}^{\text{XC}} \quad (38)$$

where

$$K_{ru,tq}^{\text{C}} = \iint \phi_r^*(1) \phi_u(1) \frac{1}{r_{12}} \phi_t^*(2) \phi_q(2) dv_1 dv_2 \quad (39)$$

whereas

$$K_{ru,tq}^{\text{XC(HF)}} = - \iint \phi_r^*(1) \phi_q(1) \frac{1}{r_{12}} \phi_t^*(2) \phi_u(2) dv_1 dv_2 \quad (40)$$

for Hartree–Fock exchange correlation and

$$K_{ru,tq}^{\text{XC(DFT)}} = \delta(m_{sr}, m_{su}) \delta(m_{st}, m_{sq}) \int \phi_r^*(\vec{r}_1) \phi_u(\vec{r}_1) [f^{(m_{sr}, m_{st})}(\rho^0)] \phi_t^*(\vec{r}_1) \phi_q(\vec{r}_1) d\vec{r}_1 \quad (41)$$

for DFT exchange correlation. In (41), $m_{sr} = 1/2$ for a spin orbital $\phi_r(1)$ of α -spin whereas $m_{sr} = -1/2$ for a spin orbital $\phi_r(1)$ of β -spin. In addition, the kernel $f^{(\tau, v)}(\rho^0)$ is the second functional derivative of E_{XC} with respect to ρ_α and ρ_β

$$f^{\tau, v}(\rho_\alpha^0, \rho_\beta^0) = \left(\frac{\delta^2 E_{\text{XC}}}{\delta \rho_\tau \delta \rho_v} \right)_0 \quad \tau = \alpha, \beta ; v = \alpha, \beta. \quad (42)$$

Finally $\varepsilon_i^0, \varepsilon_a^0$ in (37) are the ground state orbital energies of, respectively, $\phi_i(1)$ and $\phi_a(1)$.

In CV(2)-DFT [144], we seek points on the energy surface $E_{\text{KS}}[\rho']$ such that $\Delta E_{\text{KS}}[\Delta\rho'] = E_{\text{KS}}[\rho'] - E_{\text{KS}}[\rho^0]$ represents a transition energy. Obviously, a direct optimization of $\Delta E_{\text{KS}}[\Delta\rho']$ without constraints will result in $\Delta E_{\text{KS}}[\Delta\rho'] = 0$ and $U = 0$. We [144] now introduce the constraint that the electron excitation must represent a change in density $\Delta\rho'$ where one electron in (36) is transferred from the occupied space represented by $\Delta\rho_{\text{occ}} = -\sum_{ija} U_{ai} U_{aj}^* \varphi_i(1') \varphi_j^*(1)$ to the virtual space represented by $\Delta\rho_{\text{vir}} = \sum_{iab} U_{ai} U_{bi}^* \varphi_a(1') \varphi_b^*(1)$. An integration of $\Delta\rho_{\text{occ}}$ and $\Delta\rho_{\text{vir}}$ over all space affords $-\Delta q_{\text{occ}} = \Delta q_{\text{vir}} = \sum_{ai} U_{ai} U_{ai}^*$. We shall thus introduce the constraint $\sum_{ai} U_{ai} U_{ai}^* = 1$. Constructing next the Lagrangian $L = E_{\text{KS}}[\rho'] + \lambda(1 - \sum_{ai} U_{ai} U_{ai}^*)$ with λ being a Lagrange multiplier and demanding that L be stationary to any real variation in U results in the eigenvalue equation

$$(A^{\text{KS}} + B^{\text{KS}})\vec{U}^{(I)} = \lambda_{(I)}\vec{U}^{(I)}, \quad (43)$$

where

$$A_{ai,bj}^{\text{KS}} = \delta_{ab}\delta_{ij}(\varepsilon_a^0 - \varepsilon_i^0) + K_{ai,bj}^{\text{KS}}; \quad B_{ai,bj}^{\text{KS}} = K_{ai,jb}^{\text{KS}}. \quad (44)$$

We can now from (43) determine the sets of mixing coefficients $\{\vec{U}^{(I)}; I = 1, \text{occ} \times \text{vir}\}$ that make L stationary and represent excited states. The corresponding excitation energies are given by $\lambda_{(I)}$ as it can be seen by multiplying by $\vec{U}^{(I)+}$ from the left in (43) and making use of the constraint and normalization condition $\vec{U}^{(I)+}\vec{U}^{(I)} = 1$.

Within the Tamm–Dancoff approximation [146] ($B^{\text{KS}} = 0$) (43) reduces to

$$A^{\text{KS}}\vec{U}^{(I)} = \lambda_{(I)}\vec{U}^{(I)} \quad (45)$$

which is identical in form to the equation one obtains from TDDFT in its adiabatic formulation [132–137] after applying the same Tamm–Dancoff [146] approximation.

Having determined $\vec{U}^{(I)}$ from either (43) or (45) allows us [145] now to carry out the unitary transformation of (32) to all orders. The resulting occupied excited state orbitals are given by [145]

$$\varphi'_j = \cos[\eta_j]\varphi_j^o + \sin[\eta_j]\varphi_j^v; j = 1, \text{occ}, \quad (46)$$

here φ_j^o and φ_j^v are according to the corresponding orbital theory of Hall and Amos²⁷ eigenvectors to, respectively, D_{occ} and D_{vir} with the same eigenvalues γ_i where $(D_{\text{occ}}^2)_{ij} = \sum_a^{\text{vir}} U_{ai}U_{aj}$ and $(D_{\text{vir}}^2)_{ab} = \sum_i^{\text{occ}} U_{ai}U_{bi}$. Here, φ_j^o is a linear combination of occupied ground state orbitals whereas φ_j^v is a linear combinations of virtual ground state orbitals. Thus in the corresponding orbital representation [145] only one occupied orbital φ_j^o mixes with one corresponding virtual orbital φ_j^v for each occupied excited state orbital φ'_j when the unitary transformation is carried out to all orders according to (32). Martin [145] has used the representation of corresponding orbitals to analyze excitations described by TDDFT and TDHF. In his interesting analysis, $\{\varphi_j^o(1), \varphi_j^v(1)\}$ are referred to as natural transition orbitals (NTO).

The change in the density matrix $\Delta\rho^{(\infty)}$ due to a one-electron excitation takes on the compact form of

$$\begin{aligned} \Delta\rho^{(\infty)}(1, 1') &= \sum_j^{\text{occ}} \sin^2[\eta_j][\varphi_j^v(1')\varphi_j^v(1) - \varphi_j^o(1')\varphi_j^o(1)] \\ &\quad + \sum_j^{\text{occ}} \sin[\eta_j] \cos[\eta_j][\varphi_j^v(1)\varphi_j^o(1') + \varphi_j^v(1')\varphi_j^o(1)] \end{aligned} \quad (47)$$

when the unitary transformation in (32) is carried out to all orders. In (46) and (47), the scaling factor η is introduced to ensure that $\Delta\rho^{(\infty)}(1, 1')$ represent the transfer of a single electron from the occupied orbital space density $-\sin^2[\eta\gamma_j]\varphi_j^o(1')\varphi_j^o(1)$ to the virtual orbital space density $\sum_j^{\text{occ}} \sin^2[\eta\gamma_j]\varphi_j^v(1')\varphi_j^v(1)$ or

$$\sum_j^{\text{occ}} \sin^2[\eta\gamma_j] = 1. \quad (48)$$

Here, the constraint of (48) is a generalization of the corresponding second order constraint $\sum_{ai} U_{ai}U_{ai}^* = 1$ used to derive (43) and (45).

We finally get for the excitation energy including terms to all orders in U

$$\begin{aligned} \Delta E^{(\infty)} &= E_{\text{KS}}^\infty[\rho^0 + \Delta\rho^{(\infty)}] - E_{\text{KS}}[\rho^0] \\ &= -\sum_j^{\text{occ}} \sin^2[\eta\gamma_j] F_{j^o j^o}^{\text{KS}}[\rho^0 + \frac{1}{2}\Delta\rho^{(\infty)}] + \sum_j^{\text{occ}} \sin^2[\eta\gamma_j] F_{j^v j^v}^{\text{KS}}[\rho^0 + \frac{1}{2}\Delta\rho^{(\infty)}] \\ &\quad + \sum_j^{\text{occ}} \cos[\eta\gamma_j] \sin[\eta\gamma_j] F_{j^o j^v}[\rho^0 + \frac{1}{2}\Delta\rho^{(\infty)}] \\ &\quad + \sum_j^{\text{occ}} \cos[\eta\gamma_j] \sin[\eta\gamma_j] F_{j^v j^o}[\rho^0 + \frac{1}{2}\Delta\rho^{(\infty)}] + O^{[3]}(\Delta\rho^{(\infty)}). \end{aligned} \quad (49)$$

Here, (49) is derived by Taylor expanding [54] $E_{\text{KS}}^\infty[\rho^0 + \Delta\rho^{(\infty)}]$ and $E_{\text{KS}}[\rho^0]$ from the common intermediate density $\rho^0 + 1/2\Delta\rho^{(\infty)}$. Further, $F^{\text{KS}}[\rho^0 + 1/2\Delta\rho^{(\infty)}]$ is the Kohn–Sham Fock operator defined with respect to the intermediate Kohn–Sham density matrix $\rho^0 + 1/2\Delta\rho^{(\infty)}$, whereas $F_{pq}^{\text{KS}}[\rho^0 + 1/2\Delta\rho^{(\infty)}]$ is a matrix element of this operator involving the two orbitals ϕ_p, ϕ_q . The expression in (49) is exact to third order in $\Delta\rho^{(\infty)}$, which is usually enough [54]. However, its accuracy can be extended to any desired order in $\Delta\rho^{(\infty)}$ [54].

The energy expression in (49) is perturbative in the sense that we make use of a U matrix optimized with respect to the second-order energy expression of (37). We refer to this method as $\text{CV}(\infty) - \text{DFT}$ [145]. We shall now seek ways in which to find vectors $\vec{U}_{(\infty)}^{(l)}$ that optimize $E_{\text{KS}}^\infty[\rho^0 + \Delta\rho^{(\infty)}(U)]$. To this end, we can start with $\vec{U}_{(2)}^{(l)} = \vec{U}^{(l)}$ found from (45). Let us call this solution set U^0 . We can now carry out a Taylor expansion

$$\begin{aligned} E^{(\infty)}(\rho^0 + U) &= E^{(\infty)}(\rho^0 + U^0) + \sum_{ai} \left(\frac{dE^{(\infty)}}{dU_{ai}} \right)_0 \Delta U_{ai} \\ &\quad + \frac{1}{2} \sum_{ai} \sum_{bj} \left(\frac{d^2 E^{(\infty)}}{d^2 U_{ai} U_{bj}} \right)_0 \Delta U_{ai} \Delta U_{bj} \\ &= E^{(\infty)}(\rho^0 + U^0) + \sum_{ai} g(U^0)_{ai} \Delta U_{ai} + \frac{1}{2} \sum_{ai} \sum_{bj} H(U^0)_{ai,bj} \Delta U_{ai} \Delta U_{bj} + O^{(3)}[\Delta U]. \end{aligned} \quad (50)$$

Here, the gradient, \vec{g} , evaluated at U^0 has matrix elements given by

$$\begin{aligned} g(U^0)_{ai} &= \left(\frac{dE^{(\infty)}}{dU_{ai}} \right)_0 = \sum_{\sigma}^{\alpha,\beta} \left(\frac{\partial E}{\partial \rho_{\sigma}} \right)_0 \left(\frac{\partial \rho_{\sigma}}{dU_{ai}} \right)_0 \\ &= \sum_{\sigma}^{\alpha,\beta} \int \hat{F}_{\sigma}^{\text{KS}}[(U^0)] \left(\frac{\partial \rho_{\sigma}}{dU_{ai}} \right)_0 dv_1. \end{aligned} \quad (51)$$

Furthermore the Hessian $\vec{H}(U^0)$ evaluated at U^0 has matrix elements given by

$$\begin{aligned} H(U^0)_{ai,bj} &= \left(\frac{d^2 E^{(\infty)}}{dU_{ai} dU_{bj}} \right)_0 = \frac{d}{dU_{bj}} \left(\frac{dE^{(\infty)}}{dU_{ai}} \right) = \frac{d}{dU_{bj}} \sum_{\sigma}^{\alpha,\beta} \left(\frac{\partial E^{(\infty)}}{\partial \rho_{\sigma}} \right)_0 \left(\frac{\partial \rho_{\sigma}}{\partial U_{ai}} \right)_0 \\ &= \sum_{\sigma}^{\alpha,\beta} \sum_{\tau}^{\alpha,\beta} \left[\iint \left(\frac{\partial \rho_{\sigma}(1)}{\partial U_{bj}} \right)_0 \frac{1}{r_{12}} \left(\frac{\partial \rho_{\tau}(2)}{\partial U_{ai}} \right)_0 dv_1 dv_2 \right. \\ &\quad \left. + \int f^{\sigma\tau} \left[\rho(U^0) \right] \left(\frac{\partial \rho_{\sigma}}{\partial U_{bj}} \right)_0 \left(\frac{\partial \rho_{\tau}}{\partial U_{ai}} \right)_0 dv_1 + \sum_{\sigma}^{\alpha,\beta} \int F_{\sigma}^{\text{KS}} \left[\rho(U^0) \right] \left(\frac{\partial^2 \rho_{\sigma}}{\partial U_{ai} \partial U_{bj}} \right)_0 dv_1 \right. \\ &\quad \left. \cong \sum_{\sigma}^{\alpha,\beta} \sum_{\tau}^{\alpha,\beta} \left\{ F_{\tau}^{\text{KS}} \left[\rho(U^0) \right] + \left(\frac{\partial \rho_{\sigma}}{\partial U_{bj}} \right)_0 \right\} - F_{\tau}^{\text{KS}} \left[\rho(U^0) \right] \right\} \left(\frac{\partial \rho_{\tau}}{\partial U_{ai}} \right)_0 dv_1 \\ &\quad \left. + \sum_{\sigma}^{\alpha,\beta} \int F_{\sigma}^{\text{KS}} \left[U^0 \right] \left(\frac{\partial^2 \rho_{\sigma}}{\partial U_{ai} \partial U_{bj}} \right)_0 dv_1. \right. \end{aligned} \quad (52)$$

The calculation of \vec{g} and $\vec{H}(U^0)$ requires closed form expressions for $d\rho_{\sigma}^{(\infty)} \times (1, 1')/dU_{ai}$ and $d^2 \rho_{\sigma}^{(\infty)}(1, 1')/dU_{ai} dU_{bj}$ [145]. Also required are F_{pq}^{KS} and $K_{rv,st}$ integrals already available in standard DFT programs. We can now from (50) obtain the optimal step within the quadratic region

$$\Delta U_{ai} = - \sum_{bj} (H^{-1})_{ai,bj} g_{bj} \quad (53)$$

Next, in order to satisfy (48), we must scale ΔU from (53) to obtain $U' = \eta(U^0 + \Delta U)$. Here η is determined by substituting $\eta(U^0 + \Delta U)$ into (48). In addition, U' must be orthogonal to all previously found solutions $\{\vec{U}_{(\infty)}^{(K)}; K = 1, I-1\}$. Thus, we obtain a new solution U''

$$U'' = U' - \sum_K^{I-1} \langle U' | U^{(K)} \rangle / |U^{(K)}| \quad (54)$$

After having calculated U'' from (54), we now set $U^0 = U''$ and go back to (50) for another iteration. The procedure is continued until $|U^0 - U''|$ is smaller than a certain threshold. After that, the search might be extended to excited state $I + 1$.

We have already seen that adiabatic TD-DFT within the Tamm–Dancoff approximation is equivalent to CV(2) with $B^{\text{KS}} = 0$. Another scheme that has been used in the past is ΔDFT [36, 113–116] where one generates new “excited state” KS-Slater determinants from the ground state determinant by substituting one of the occupied ground state KS-orbitals $\{\phi_i(1); i = 1, \text{occ}\}$ with a virtual KS-orbitals $\{\phi_a(1); a = 1, \text{vir}\}$. An evaluation of the energy of the new determinant followed by subtraction of the ground state energy makes it possible to determine the excitation energy $\Delta E_{i \rightarrow a}^{\Delta\text{DFT}}$. In relation to CV(n)-DFT, the ΔDFT scheme is equivalent to applying the following approximations in (50):

$$(U^0)_{bj} = (U^0)_{ai} \delta_{ab} \delta_{ij}; \quad \Delta U = 0, \quad (55)$$

where $\Delta U = 0$ indicates that ΔDFT is a non-SCF method. The resulting excitation energy is given as

$$\begin{aligned} \Delta E_{i \rightarrow a}^{\Delta\text{DFT}} &= E^{(\infty)}(\rho^0 + U^0) - E^{(\infty)}(\rho^0) \\ &\cong \int F^{\text{KS}} \left[\rho^0 + \frac{1}{2} U_{ai} U_{ai} [\phi_a \phi_a - \phi_i \phi_i] \right] U_{ai} U_{ai} [\phi_a \phi_a - \phi_i \phi_i] dV_1 \\ &= \varepsilon_a^0 - \varepsilon_i^0 + \frac{1}{2} K_{aa,aa}^{\text{KS}} + \frac{1}{2} K_{ii,ii}^{\text{KS}} - K_{ii,aa}^{\text{KS}}, \end{aligned} \quad (56)$$

where we in the last line has used that $U_{ai} = 1$.

Another method mentioned above is the ΔSCF scheme. In this method [36, 113–116], one promotes as in ΔDFT an electron from an occupied ground state KS-orbital $\{\phi_i(1); i = 1, \text{occ}\}$ to a virtual KS-orbital $\{\phi_a(1); a = 1, \text{vir}\}$ by introducing $(U^0)_{bj} = (U^0)_{ai} \delta_{ab} \delta_{ij}$. However, in contrast to ΔDFT where $\Delta U = 0$, the ΔSCF scheme updates ΔU and $\Delta \rho^{(\infty)}(1, 1')$ of (47) with the help of the diagonal part of the Hessian, or an approximation, as $\Delta U_{bj} = -g_{bj}[\rho^0 + \Delta \rho^{(\infty)}] H_{bj,bj}^{-1}$ ($b=1, \text{vir}; j=1, \text{occ}$) until self-consistency when $g_{bj}[\rho^0 + \Delta \rho^{(\infty)}] = 0$. The resulting excitation energy is given by

$$\Delta E_{a \rightarrow i}^{\Delta\text{SCF}} = \int F^{\text{KS}} \left[\rho^0 + \frac{1}{2} \Delta \rho^{(\infty)} \right] \Delta \rho^{(\infty)} dV_1 \quad (57)$$

As in ΔDFT , “ a ” and “ i ” in U_{ai} belongs to the same symmetry representation. This can be seen by realizing that the initial guess for $\Delta \rho^{(\infty)}$ is $\psi_a \psi_a - \psi_i \psi_i$ which is totally symmetric. Thus, in subsequent updates $\Delta U_{bj} = -g_{bj}[\rho^0 + \Delta \rho^{(\infty)}] H_{bj,bj}^{-1}$ we have that $\Delta U_{bj} = 0$ if “ b ” and “ j ” in U_{bj} belongs to different representations. That is clearly a limitation compared to TDDFT where $\Delta U_{bj} \neq 0$ provided that

$\Delta\rho^{(\infty)}$ has contributions from U_{ck} where the direct product between “bj” and “ck” has a contribution from the totally symmetric representation.

On the other hand, Δ DFT and Δ SCF includes the higher order “self-interaction terms” missing in TDDFT for a qualitatively correct description of charge transfer transitions. Furthermore, the orbitals in Δ SCF are specifically optimized for the $i \rightarrow a$ transition. Unfortunately, the unconstrained optimization applied in traditional Δ SCF often leads to the variational collapse of the energy for higher lying excited states unto the energy of lower lying excited states. Finally, in Δ SCF we start with $U_{ai} = 1$. As orbitals of different symmetry are not allowed to mix, this ensures that the occupation of orbitals belonging to a certain symmetry representation in Δ SCF remains the same throughout the SCF procedure from the initial Δ DFT step ($U_{ai} = 1$) to the converged result.

3.2 *Different Hartree–Fock and Post-Hartree–Fock Methods Used in the Study of Excited States*

The approximate LCAO methods have all been applied to the excited states of transition metal complexes. This is the case for the schemes based on the Wolfberg–Helmholtz approximation [13] (WH) as well as the more quantitative CNDO, INDO and NDDO methods [21]. Results from the Extended Hückel [14] and Fenske–Hall [18] approaches where the WH approximation is applied can only be considered qualitative [24]. However, in contrast to ligand field theory [5], these schemes describe also CT between metals and ligands as well as ligand to ligand transitions [147]. Of the differential overlap methods [21], the most widely used for excited states of transition metals has been the ZINDO [27] scheme by Zerner. However, the predicted excitation energies depend heavily on the exponents chosen for the minimal Slater- type basis set. Applications of the ab initio HF method to the absorption spectra of transition metal complexes such as MnO_4^- [95–100] became possible in the early 1970s [29, 30]. However, the results were often disappointing. This is not surprising since the correlation energy neglected by HF can be quite different for the ground and excited states.

Post-Hartree–Fock methods were in the 1970s and 1980s mostly applied to diatomic molecules with one or two transition metals where comparison could be made to high-resolution gas phase experiments [148]. As computers became faster, the applications were extended to larger systems. However, coupled cluster and MCSCF schemes that are best suited for the study of transition metal complexes in their excited states scales as $(n_e)^6$ or worse. This puts severe limits on the size of the studied systems even today. Among the CC methods, the iterative coupled cluster approach including connected triples (CC3) [149] as well as the equation of motion (EOM) [150] affords the most accurate results for systems, where Hartree–Fock gives a reasonable description of the ground state [151]. Alternatives that also works for cases where Hartree–Fock is a poor zero-order description are

the symmetry adapted cluster/configuration interaction (SAC-CI) method [94] and schemes based on MCSCF such as the CASSCF [90] and its CASPT2 extension [91]. Especially CASPT2 has been employed extensively in studies of transition metal systems by Björn Ross and collaborators [152, 153].

3.3 Theoretical Studies on the Absorption Spectrum of Permanganate and Related Tetroxo Complexes

Permanganate has served as a testing ground and litmus test for many computational methods as they emerged over the past 60 years. Of particular interest has been the absorption spectrum and we shall in this section discuss the performance of a number of the methods described above.

The low temperature and high-resolution absorption spectrum of permanganate as recorded by Holt and Ballhausen [12] is shown in Fig. 4. The first allowed band (I) starting at 2.27 eV ($18,300\text{ cm}^{-1}$) has a well-resolved vibronic structure. It is followed by a featureless shoulder (II) at 3.47 eV ($28,000\text{ cm}^{-1}$) and another strong band (III) at 3.99 eV ($32,000\text{ cm}^{-1}$) with a clear vibronic fine structure. We finally have a strong featureless band (IV) at 5.45 eV ($43,960\text{ cm}^{-1}$).

Wolfberg and Helmholz [13] put their newly developed LCAO method (1952) to the test by calculating the first two excitation energies of MnO_4^- . They had in their calculation an inversion of the order of the first two virtual orbitals of Fig. 2 with $\varepsilon_{3t_2} < \varepsilon_{2e}$. This ordering is at odds with ligand field theory and lead to the controversial assignment of the first two bands as (I): (b) $t_1 \rightarrow 3t_2$ and (II): (d) $2t_2 \rightarrow 3t_2$, Table 7. The ligand field ordering was subsequently recovered in other semi-empirical calculations [161–167]. However, these schemes are too parameter dependent to afford a reliable detailed assignment [167]. The introduction by Hillier and Saunders [29] as well as Veillard [30] of first principle Hartree Fock programs lead shortly after to a series of ab initio HF calculations on the electronic

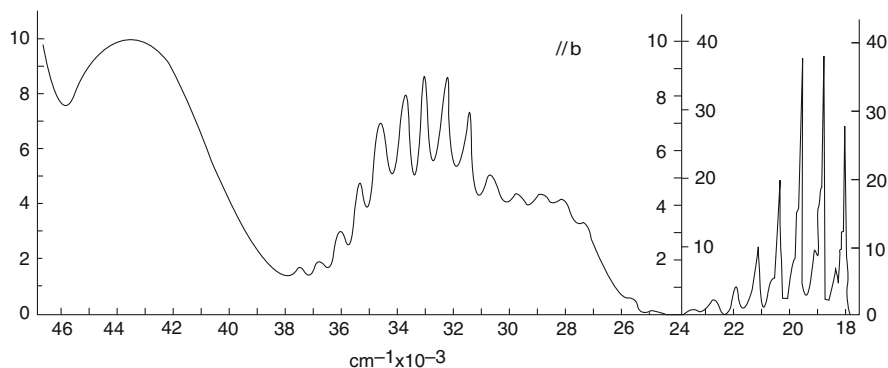


Fig. 4 Experimental absorption spectrum of MnO_4^- from Holt and Ballhausen [12]

Table 7 Calculated^a and experimental excitation energies^b for MnO_4^-

WH ^c	HF ^d	EOM ^e	STEOM ^f	HF + CI ^g	SAC-CI ^h	SW-X α ⁱ	X α ^j	LDA ^k	TDDFT ^l	^c Exp
1.68 ^m	1.04 ⁿ	2.24 ⁿ	1.92 ⁿ	2.6 ⁿ	2.48 ⁿ	2.3 ⁿ	2.48 ⁿ	2.71 ⁿ	2.87 ⁿ	2.27
2.78 ^a	2.54 ^o	3.60 ^o	3.08 ^m	4.1 ^o	3.96 ^m	3.3 ^o	3.96 ^o	4.02 ^o	3.89 ^o	3.47
	2.94 ^m	3.67 ^m	3.51 ^o	4.5 ^m	4.15 ^o	4.7 ^m	4.15 ^m	4.22 ^m	4.77 ^m	3.99
	4.77 ^p	5.80 ^a		6.1	5.82 ^{a,b}	5.3 ^a	5.65 ^a	5.70 ^a	5.77 ^a	5.45

^a $2t_2 \rightarrow 3t_2$ ^beV^c[12]^d[97]^e[154]^f[155]^g[98, 99]^h[156]ⁱ[157]^j[158]^k[159]^l[160]^m $t_1 \rightarrow 3t_2$ ⁿ $t_1 \rightarrow 2e$ ^o $2t_2 \rightarrow 2e$ ^p $1t_2 \rightarrow 2e$ [13]

spectrum of MnO_4^- [97–102]. While the first calculations were limited to small basis sets, Hsu [97] et al. published in 1976 a basis set limit calculation, Table 7. Their results are only in fair agreement with experiment, Table 7. There have finally been four post-HF studies. The first two by Nooijen employ EOM-CCSD [154] and STEOM [155], whereas the third by Johansen and Retrup [98] is based on HF augmented by single and double excitations (HF + CI). The fourth by Nakatsuji [156] et al. employs SAC + CI. All assign (I) to $t_1 \rightarrow 2e$. However, the closely spaced next two bands are assigned as (II): $t_1 \rightarrow 3t_2$, (III): $2t_2 \rightarrow 2e$ for SAC + CI and STEOM with (II): $2t_2 \rightarrow 2e$, (III): $t_1 \rightarrow 3t_2$ for HF + CI and EOM. We shall refer to these assignments as the bc and cb orderings, respectively. It is obvious that all four methods are able to reach semi-quantitative accuracy. However they are likely not accurate enough to conclusively settle which of the two orderings (bc or cb) is the correct one. It would be very interesting to have a study of permanganate based on CASPT2

Also shown in Table 7 are results based on DFT. The three first entries are due to Δ SCF calculations using the SW-X α [157], the X α [158] and the LDA [159] approaches of which the last provides full resolution of all space and spin multiplets. The results are quite similar and in reasonable agreement with experiment. All three methods point to the cb ordering. We finally have a number of TDDFT [160, 168, 169] calculations with the one by Neugebauer et al. [159] shown in Table 7. TDDFT allows in principle one-electron excitations such as $t_1 \rightarrow 3t_2$ and $2t_2 \rightarrow 2e$ to mix. Nevertheless, all TDDFT calculations are consistent with a cd ordering similar to Δ SCF although some mixing of $t_1 \rightarrow 3t_2$ and $2t_2 \rightarrow 2e$ takes place in II and III.

Neugebauer et al. [160] have recently simulated the absorption spectrum for permanganate by including the vibronic fine structure as shown in Fig. 5.

Their simulation catches the main features of the experimental spectrum in Fig. 4. It is also argued by the authors that the assignment of bands in terms of one electron transitions such as $t_1 \rightarrow 3t_2$ and $2t_2 \rightarrow 2e$ is too simplistic as these transitions are mixed by vibronic coupling. More quantitative calculations are needed to see whether this in fact is the case for permanganate.

We finally have in Table 8 calculated excitation energies for a number of tetroxo systems by SAC-CI [170] and three DFT-based methods of which the first two are Δ SCF schemes [158, 159] and the last an adiabatic TDDFT approach [171]. All schemes find the first band to be due to $t_1 \rightarrow 2e$ with the exception of MoO_4^{2-} where SAC-CI finds the assignment $t_1 \rightarrow 3t_2$. For the 4d samples RuO_4 , MoO_4^{2-} and the 5d complex OsO_4 , the general assignment for II and III is $2t_2 \rightarrow 2e$ and $t_1 \rightarrow 3t_2$, respectively, corresponding to the cb ordering with the exception of MoO_4^{2-} for the case of SAC-CI. The cb ordering is to be expected for 4d and 5d complexes where the ligand field splitting $\varepsilon_{3t_2} - \varepsilon_{2e}$ is large. For the 3d systems such as CrO_4^{2-} and MnO_4^- , the ligand splitting $\varepsilon_{3t_2} - \varepsilon_{2e}$ is smaller resulting in quite similar calculated energies for $2t_2 \rightarrow 2e$ and $t_1 \rightarrow 3t_2$ as well as a close experimental positions of bands II and III. It can be seen that SAC-CI for 3d systems give rise to the bc ordering whereas all DFT methods point to the cb ordering.

We will conclude by stating that there is general consensus on the assignment of the first three bands for 4d and 5d tetroxo complexes. However, for the 3d tetroxo complexes more work has to be done before a definitive assignment can be given of bands II and III. This is a somewhat sobering conclusion given the fact that the work on permanganate has been ongoing for more than 60 years.

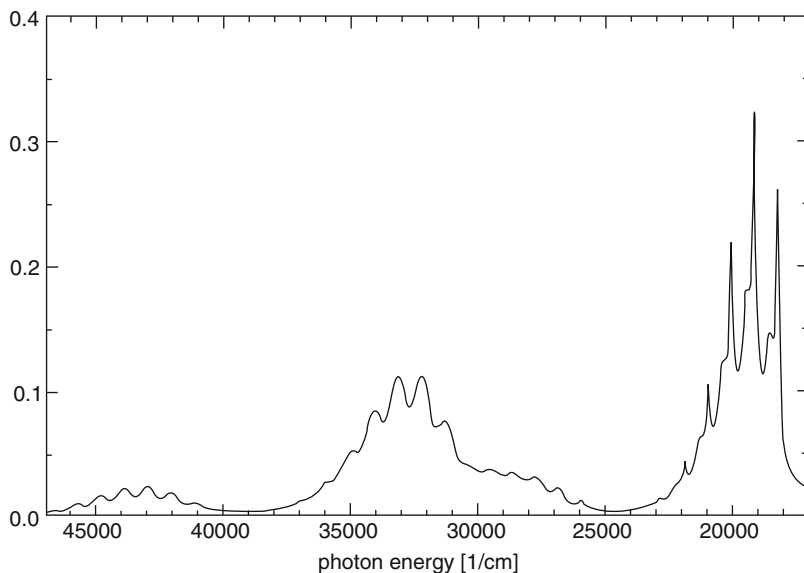


Fig. 5 Simulated absorption spectrum for permanganate due to Neugebauer et al. [160]

Table 8 Calculated^a and experimental excitation energies for some tetroxo complexes

Complex	SAC-CI ^b	$\Delta\text{SCF}(X\alpha)^c$	$\Delta\text{SCF}(\text{LDA})^d$	^e TDDFT	^e Exp
CrO_4^{2-}	3.41 ^f	3.30 ^f	3.64 ^f	3.79 ^f	3.32
	4.16 ^g	4.58 ^h	4.83 ^h	4.67 ^h	4.53
	4.51 ^h	4.90 ^g	5.18 ^g	5.39 ^g	4.86
MoO_4^{2-}	4.37 ^g	5.17 ^f	5.40 ^f	5.66 ^f	5.34
	5.14 ^h	5.84 ^h	5.89 ^h	6.15 ^h	5.95
	5.52 ^f	7.16 ^g	7.22 ^g		
MnO_4^-	2.57 ^f	2.48 ^f	2.71 ^f	2.87 ^f	2.27
	3.58 ^g	3.96 ^h	4.02 ^h	3.89 ^h	3.47
	3.72 ^h	4.15 ^g	4.22 ^g	4.77 ^g	3.99
RuO_4	3.22 ^f	3.02 ^f	3.28 ^f	3.69 ^f	3.22
	4.55 ^h	3.81 ^h	4.00 ^h	4.51 ^h	4.09
	5.23 ^g	4.56 ^g	5.06 ^g	5.87 ^g	5.03
OsO_4	3.90 ^f	-	4.29 ^f	5.06 ^f	4.34
	5.46 ^h	-	4.75 ^h	5.81 ^h	5.21
	6.41 ^g	-	6.76 ^g	7.11 ^g	5.95

^aeV^b[170]^c[158]^d[159]^e[171]^f $t_1 \rightarrow 2e$ ^g $t_1 \rightarrow 3t_2$ ^h $2t_2 \rightarrow 2e$

3.4 Theoretical Studies on the Magnetic Circular Dichroism Spectrum of Permanganate and Related Tetroxo Complexes

Magnetic circular dichroism (MCD) spectroscopy [171, 172] involves the measurement of the difference in absorption of left and right circularly polarized light in the presence of a magnetic field. An MCD signal can be negative or positive and MCD spectra can provide useful information about the nature of the excited states of a molecule that may not be available from the positive absorption spectrum. MCD spectroscopy is particularly useful when degenerate states are present since the applied magnetic field then will perturb the energies of these states to first order.

The observed MCD spectrum can be expressed in terms of three parameters or terms (A_J , B_J and C_J) as

$$\text{MCD}(\hbar\omega) = \chi\hbar\omega B \sum_J A_J \left(-\frac{\partial f_J(\hbar\omega - \hbar\omega_J)}{\partial \hbar\omega} \right) + \left(B_J + \frac{C_J}{kT} \right) f_J(\hbar\omega - \hbar\omega_J),$$

where $\hbar\omega$ is the energy of the incident light, $\hbar\omega_J$ is the excitation energy to state J , B is the amplitude of the applied magnetic field, k is Boltzmann's constant, T is the temperature and f_J is a band shape function, whereas χ is a collection of constants

and experimental parameters. The parameters A_J , B_J and C_J can on the one hand be calculated from first principle and on the other hand be extracted from the experimentally measured MCD intensity $MCD(\hbar\omega)$. We shall here exclusively be interested in the contribution from A_J as the excited states in tetroxo systems to which transitions are allowed are degenerate and of T_2 symmetry.

The presence of an intense A term is a strong indication that the excited state of a transition is spatially degenerate thereby helping to assign that transition and perhaps providing evidence as to the overall symmetry of the molecule under investigation. In addition to A_J , the ratio A_J/D_J is often obtained from an experimental spectrum. Here, D_J is the dipole strength of the transition to state J in the absorption spectrum and is closely related to the oscillator strength. The ratio A_J/D_J is of interest because it can be directly related to the magnetic moment of the excited state and is less subject to environmental effects than A_J (Table 9).

We present in Fig. 6 the simulated [171] and experimental MCD spectra for VO_4^{3-} , CrO_4^{2-} and MnO_4^- . Except for a blue shift, the agreement between the calculated and observed spectra is rather good. For all three systems, the first band gives rise to a negative A term and a negative A_J/D_J ratio in agreement with experiment. For CrO_4^{2-} and MnO_4^- theory predicts that the second band should be weak whereas the third band exhibits a strong positive A term with a large positive A_J/D_J ratio, in good agreement with experiment. The predicted MCD spectrum involving bands II and III is also in good agreement with experiment for VO_4^{3-} .

The good fit between theory and experiment for CrO_4^{2-} and MnO_4^- in the simulation of their MCD spectra provides perhaps the strongest support for the assignment II: $2t_2 \rightarrow 2e$ and III: $t_1 \rightarrow 3t_2$ provided to date for these two systems.

Table 9 Calculated^a and experimental excitation energies, A_J terms^b and A_J/D_J ^b parameters

		Theory		^a Exp		
		A_J	A_J/D_J	${}^c\hbar\omega_J$	A_J	A_J/D_J
VO_4^{3-}	${}^c\hbar\omega_J$					
	4.66 ^d	-0.04	-0.37	4.58	-0.29	-0.46
	5.38 ^e	0.0003	0.06	5.58	+	+
CrO_4^{2-}	5.87 ^f	0.042	0.61	6.15		
	3.79	-0.057	-0.53	3.32	-0.191	-0.58
	4.67	0.0016	0.08	4.53		
MnO_4^-	5.39	0.063	0.85	4.86	0.195	0.63
	2.87 ^d	-0.061	-0.66	2.27	-0.085	-0.48
	3.89 ^e	0.0025	0.10	3.47	-	-
	4.77 ^f	0.071	0.97	3.99	0.155	0.86

^a[171]

^bAll values in au

^ceV

^d $t_1 \rightarrow 2e^f t_1 \rightarrow 3t_2$

^e $2t_2 \rightarrow 2e$

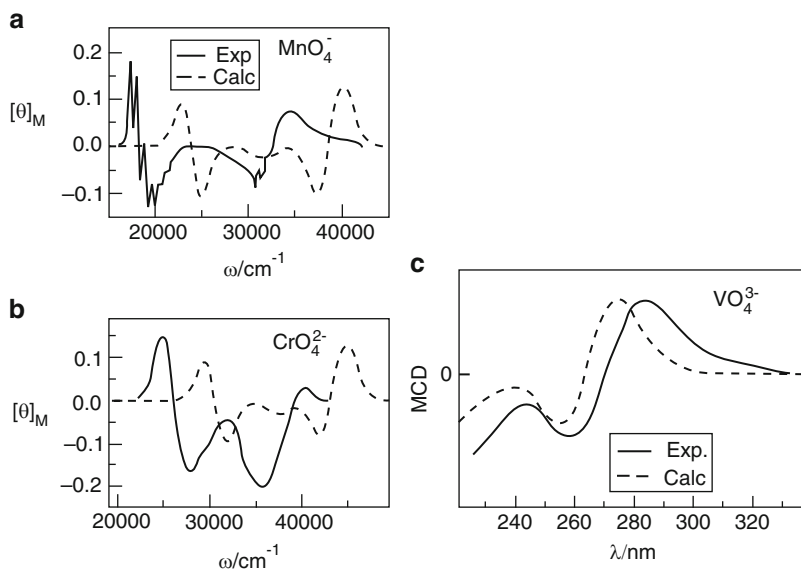


Fig. 6 Simulated and observed MCD spectra for VO_4^{3-} , CrO_4^{2-} and MoO_4^{3-} from [171]

4 Concluding Remarks

Some 60 years have passed since the first LCAO calculations on transition metal complexes appeared [13]. Electronic structure theory is now at the point where it is possible to describe the potential energy surface (PES) of a gas phase molecule containing up to 20 atoms with great accuracy using high level wave function methods such as CCSD(T) (ground state) or EOM/CASSPT2/SAC-CI (excited states). For larger systems, acceptable accuracy can be obtained by DFT (ground state) or TD-DFT/ Δ SCF-DFT (excited states). Great strides have also been taken in describing the PES for reactions on surfaces in the interface between gas phase and solid state. Here, DFT will continue to be the electronic structure theory of choice. Of special importance for transition metals is the development of methods that include relativistic effects since they are required to describe periodic trends correctly within a triad of transition metals. As hardware becomes faster larger molecules can be treated with higher accuracy using existing methodology. Known methods are also likely to become faster by neglecting interactions between fragments in large molecules that are “far apart”. In this way, most methods will eventually become linear in the number of atoms if this number is large enough. It is finally possible that further progress in approximate DFT will result in new methods with the same accuracy as highly correlated wave functions and speeds still comparable to GGA-DFT.

Many chemical systems of interest have large bulky groups that exert steric pressure on the reactive centre as an essential part of how they function. For such

systems increasing use will be made of dual- or multi-level approaches in which the steric bulk is treated at a lower level of theory than the reactive system. The reason that one would like to treat bulky groups by simple theories such as molecular mechanics (MM) is not only that they have a large number of electrons but also (rather) that they potentially possess a formidable number of conformations. The many conformations make it difficult (expensive) to determine the global energy minimum even with MM.

Solvent effect can have a profound effect on chemical reactions, yet we do not at the moment have a proven methodology (as in the case of electronic structure theory) that by well-known routes can converge to chemical accuracy. Continuum methods are going to carry the bulk of the workload in the foreseeable future. However, it will be one of the major challenges within the next decade to develop solvation theories that by standard procedures will converge to chemical accuracy. Such methods are likely to combine explicit solvation for the first few solvation shelves with bulk descriptions (continuum or mean-field) for the remaining part of the solvent.

Turning next to dynamics on the PES and calculations of reaction rates, one might expect that these rates for the majority of cases will be determined with the help of Eyring's transition state method. To this end, locating saddle points on the PES is still time consuming in terms of manpower, and more systematic and automated procedures would be welcome.

The number of studies of inorganic reaction mechanisms by theoretical methods has increased drastically in the last decade. The studies cover ligand substitution reactions, insertion reactions oxidative addition, nucleophilic and electrophilic attack as well as metallacycle formation and surface chemistry, in addition to homogeneous and heterogeneous catalysis as well as metalloenzymes. We can expect the modeling to increase further both in volume and in sophistication [173].

Acknowledgement T.Z. would like to thank the Canadian government for a Canada research chair in theoretical inorganic chemistry and NSERC for financial support. Thanks also go to Drs. M. Seth and M. Krykunov for many interesting discussions.

References

1. Becquerel J (1929) *Z Phys* 58:205
2. Bethe H (1929) *Ann Phys* 3:133–208
3. Van Vleck JH (1935) *J Chem Phys* 3:803–806
4. Orgel LE (1960) *An introduction to the transition-metal chemistry: ligand-field theory*. Methuen, London
5. Ballhausen CJ (1962) *Introduction to ligand field theory*. McGraw-Hill, New York
6. Mulliken RS (1932) *Phys Rev* 40:55
7. Ilse FE, Hartmann H (1951) *Z Naturforsch* 6a:751
8. Roothan CCJ (1951) *Rev Mod Phys* 23:69–89
9. Hall GG (1951) *Proc R Soc Lond A* 205:541–552
10. Bursten BE, Drummon FF, Li J (2003) *Faraday Discuss* 124:1

11. Teltow J (1938) *Z Phys Chem B* 40:397
12. Holt SL, Ballhausen CJ (1967) *Theor Chim Acta* 7:313
13. Wolfsberg M, Helmholz LJ (1952) *J Chem Phys* 20:837
14. Hoffmann R (1963) *J Chem Phys* 39:1397–1412
15. Hoffmann R (1982) *Angew Chem Int Ed Engl* 21:711–724
16. Albright TA, Burdett JK, Whangbo MH (1985) *Orbital interactions in chemistry*. Wiley, New York
17. Burdett JK (1980) *Molecular shapes: theoretical models of inorganic stereochemistry*. Wiley, New York
18. Hall MB, Fenske RF (1972) *Inorg Chem* 11:768–775
19. Hall MB (1978) *J Am Chem Soc* 100:6333–6338
20. Pople JA, Santry DP, Segal GA (1965) *J Chem Phys* 43:S129
21. Dewar MJS, Zoebisch EG, Healy EF, Stewart JJP (1985) *J Am Chem Soc* 107:3902
22. Stewart JJP (1989) *J Comput Chem* 10:221
23. Dewar MJS, Thiel W (1977) *J Am Chem Soc* 99:4899–4907
24. Dahl JP, Ballhausen CJ (1968) *Adv Quantum Chem* 4:170
25. Ziegler T (1974) *Acta Chem Scand A* 28:29
26. Truax DR, Geer JA, Ziegler T (1973) *J Chem Phys* 59:6662
27. Zerner M (1991) In: Lipkowitz KB, Boyd DB (eds) *Reviews in computational chemistry*, vol 2. VCH, New York, p 313
28. Marynick DA, Lipscomb WN (1982) *Proc Natl Acad Sci USA* 79:1341–1345
29. Hillier IH, Saunders VR (1969) *J Chem Soc Chem Commun* 1275–1276
30. Veillard A (1969) *J Chem Soc Chem Commun* 1022–1023
31. Coutière M-M, Demuyck J, Veillard A (1972) *Theor Chim Acta* 27:281–287
32. Dirac PAM (1930) *Proc Cambridge Philos Soc* 26:376
33. Fermi E (1928) *Z Phys* 48:73
34. Thomas H (1927) *Proc Cambridge Philos Soc* 23:542
35. Slater JC (1951) *Phys Rev* 81:385
36. Ziegler T, Rauk A, Baerends EJ (1977) *Theor Chim Acta* 43:261
37. Slater JC (1974) *The self-consistent field for molecules and solids: quantum theory of molecules and solids*, vol 4. McGraw Hill, New York
38. Hohenberg P, Kohn W (1964) *Phys Rev* 136:864
39. Johnson KH (1966) *J Chem Phys* 45:3085
40. Korringa J (1947) *J Physica* 13:392
41. Case DA (1982) *Annu Rev Phys Chem* 33:151
42. Salahub DR, Messmer RP, Johnson KH (1976) *Mol Phys* 31:521
43. Ellis DE, Painter GS (1970) *Phys Rev B* 2:2887
44. Baerends EJ, Ellis DE, Ros P (1973) *Chem Phys* 2:41
45. Sambe H, Felton RH (1975) *J Chem Phys* 62:1122
46. Dunlap BI, Connolly JWD, Sabin JF (1979) *J Chem Phys* 71:4993
47. Gunnarson O, Harris J, Jones RO (1977) *Phys Rev* 15:3027
48. Becke AD (1988) *J Chem Phys* 88:2547
49. Boerrigter PM, te Velde G, Baerends EJ (1988) *Int J Quantum Chem* 33:87
50. Delley BJ (1990) *Chem Phys* 92:508
51. te Velde G, Baerends EJ (1992) *J Comput Phys* 99:84
52. Pederson MR, Ackson MRKA (1990) *Phys Rev* 41:7453
53. Delley BJ, Ellis E (1982) *J Chem Phys* 76:1949
54. Ziegler T, Rauk A (1977) *Theor Chim Acta* 46:1
55. Versluis L, Ziegler T (1988) *J Chem Phys* 88:322
56. Jacobsen H, Berces A, Swerhone DP, Ziegler T (1997) *Comput Phys Commun* 100:263–276
57. Berces A, Dickson RM, Fan L, Jacobsen H, Swerhone DP, Ziegler T (1997) *Comput Phys Commun* 100:247–262
58. Wolff SK (2005) *Int J Quantum Chem* 104:645

59. Andzelm J, Salahub DR (1986) *Int J Quantum Chem* 14:1091
60. Andzelm J (1991) In: *Density functional methods in chemistry*. Springer, New York
61. Dunlap DI, Rösch N (1990) *Adv Quantum Chem* 21:317
62. Liu WJ, Wang F, Li LM (2003) *J Theor Comput Chem* 2:257–272
63. Almlöf J, Korsel K, Faegri K Jr (1982) *J Comput Chem* 3:385
64. Horn H, Weiss H, Häser M, Ehring M, Ahlrichs R (1991) *J Comput Chem* 12:1058
65. Ahlrichs R, Tsereteli K (2001) *J Comput Chem* 23:306–309
66. Boström J, Delcey MG, Aquilante F, Serrano-Andrés L, Pedersen TB, Lindh R (2010) *J Chem Theor Comput* 6:747–754
67. Becke AD, Dickson RM (1990) *J Chem Phys* 92:3610
68. Lüthi HP, Siegbahn PEM, Almlöf J (1985) *J Phys Chem* 89:2156
69. Lüthi HP, Ammeter JA, Almlöf J, Faegri K (1982) *J Chem Phys* 77:2002
70. Rosch N, Jorg NH, Dunlap BI (1985) *NATO ASZ* 1:176
71. Dunlap BI (1986) *J Phys Chem* 90:5524
72. Antolovic A, Davidson ER (1988) *J Chem Phys* 88:4967
73. Versluis L, Ziegler T (1989) *J Am Chem Soc* 111:2018
74. Tschinke V, Ziegler T (1990) *J Chem Phys* 93:8051–8060
75. Buijse MA, Baerends EJ, Snijders JG (1989) *Phys Rev A* 40:4190–4202
76. Becke AD (1986) *J Chem Phys* 85:7184
77. Becke AD (1988) *J Chem Phys* 88:1053
78. Becke AD (1993) *J Chem Phys* 98:5648
79. Ziegler T, Tschinke V, Ursebach CJ (1987) *J Am Chem Soc* 109:4827
80. Perdew JP (1986) *Phys Rev B* 33:8822
81. Lee C, Yang W, Parr RG (1988) *Phys Rev B* 37:785
82. Sholl DS, Steckel JA (2009) *Density functional theory: a practical introduction*. Wiley, Hoboken
83. Koch W, Holthausen MC (2000) *A chemist's guide to density functional theory*. Wiley-VCH, New York
84. Burke K (2009) *The ABC of DFT*. <http://dft.uci.edu/materials/bookABCDFT/gamma/g1.pdf>
85. Perdew JP (2009) *Density functional theory*. <http://007-chbooks.blogspot.com/2009/07/density-functional-theory-john-p-perdew.html>
86. Becke AD, Johnson ER (2007) *J Chem Phys* 127:124108
87. Johnson ER, Becke AD (2009) *Can J Chem* 87:1369
88. Jensen F (2006) *Introduction to computational chemistry*, 2nd edn. Wiley, New York
89. Head-Gordon M, Pople JA, Frisch MJ (1988) *Chem Phys Lett* 153:503–506
90. Olsen J, Ross BO, Jørgensen P, Aa. Jensen HJ (1988) *J Chem Phys* 89:2185
91. Finley J, Malmqvist P-A, Roos BO, Serrano-Andrés L (1998) *Chem Phys Lett* 288:299
92. Goddard WA, Dunning TH, Hunt WJ, Hay PJ (1973) *Acc Chem Res* 6:368
93. Shaik S, Hiberty PC (2008) *A chemist's guide to valence bond theory*. Wiley-Interscience, New Jersey
94. Nakatsuji H, Hirano K (1978) *J Chem Phys* 68:2053
95. Johansen H (1972) *Chem Phys Lett* 17:569
96. Wood MH (1973) *Theoret Chim Acta* 36:309
97. Hsu H, Peterson C, Pitzer RM (1976) *J Chem Phys* 64:791
98. Rettrup S (1978) *Spin-coupled wave functions in ab initio SCF and CI calculations with application to the manganate ion*. Dissertation, The Technical University of Denmark, DK-2800 Lyngby
99. Johansen H, Rettrup S (1983) *Chem Phys* 74:77
100. Johansen H (1983) *Mol Phys* 49:1209
101. Hillier H, Saunders VR (1970) *Proc R Soc Lond A* 320:161
102. Hillier H, Saunders VR (1971) *Chem Phys Lett* 9:219
103. Buijse M, Baerends EJ (1990) *J Chem Phys* 93:4129

104. Kaupp M, Bühl M, Malkin VG (eds) (2002) Calculation of NMR and ESR parameters. Wiley-VCH, Weinheim
105. Kaupp M, Malkin OL, Malkin VG (1997) *J Chem Phys* 106:9201
106. Schreckenbach G, Ziegler T (1997) *Int J Quantum Chem* 61:899
107. Khandogin J, Ziegler T (1999) *Spectrochim Acta* 55:607
108. Malkina OL, Salahub DR, Malkin VG (1996) *J Chem Phys* 105:8793
109. Autschbach J, Ziegler T (2000) *J Chem Phys* 113:9410
110. Gaudoin R, Burke K (2004) *Phys Rev Lett* 93:173001–1
111. Oliveira LN, Gross EKV, Kohn W (1988) *Phys Rev A* 37:2821
112. Gidopoulos NI, Papaconstantinou PG, Gross EKV (2002) *Phys Rev Lett* 88:03300
113. Levy M, Nagy A (1999) *Phys Rev Lett* 83:4361
114. Slater JC, Wood JH (1971) *Int J Quantum Chem* 4S:3
115. Slater JC (1972) *Adv Quantum Chem* 6:1
116. Levy M, Perdew JP (1985) *Phys Rev A* 32:2010
117. Nagy A (1996) *Phys Rev A* 53:3660
118. Besley N, Gilbert A, Gill P (2009) *J Chem Phys* 130:124308
119. Liu TQ, Han WG, Himo F, Ullmann GM, Bashford D, Toutchkine A, Hahn KM, Noodleman L (2004) *J Phys Chem A* 108:3545–3555
120. Gavnholt J, Olsen T, Engelund M, Schiötz J (2008) *Phys Rev B* 78:075441
121. Zope R, Baruah T, Richardson S, Pederson M, Dunlap BI (2010) *J Chem Phys* 133:034301
122. Runge RE, Gross EKV (1984) *Phys Rev Lett* 52:997
123. Casida ME (1995) In: Chong DP (ed) Recent advances in density functional methods. World Scientific, Singapore, pp 155–193
124. Casida ME (1999) Workshop proceedings of the joint ITP/INT workshop on time-dependent density functional theory, 15–17 April 1999 at http://www.itp.ucsb.edu/online/tddft_c99
125. van Gisbergen SJA, Snijders JG (1995) *J Chem Phys* 103:9347
126. Petersilka M, Grossmann UJ, Gross EKV (1996) *Phys Rev Lett* 76:12
127. Bauernschmitt R, Ahlrichs R (1996) *Chem Phys Lett* 256:454
128. Stratmann RE, Scuseria GE, Frisch MJ (1998) *J Chem Phys* 109:8218
129. Helgaker T, Jørgensen P, Olsen J (2000) *Molecular electronic-structure theory*. Wiley, New York
130. Autschbach J, Ziegler T (2003) *Coord Chem Rev* 238:83
131. McWeeny R (1982) *Methods of molecular quantum mechanics*, 2nd edn. Academic, London
132. Jacquemin D, Perpète EA, Ciofini I, Adamo C, Valero R, Zhao Y, Truhlar DG (2010) *J Chem Theory Comput* 6:2071
133. Goerigk L, Grimme S (2010) *J Chem Phys* 132:184103
134. Tawada Y, Tsuneda T, Yanagisawa S, Yanai T, Hirao K (2004) *J Chem Phys* 120:8425
135. Song J-W, Watson MA, Hirao K (2009) *J Chem Phys* 131:144108
136. Schreiber M, Silva-Junior M, Sauer S, Thiel W (2008) *J Chem Phys* 128:134110
137. Stein T, Kronik L, Baer R (2010) *J Am Chem Soc* 131:2818
138. Neugebauer J, Gritsenko O, Baerends EJ (2006) *J Chem Phys* 124:214102
139. Schipper PRT, Gritsenko OV, van Gisbergen SJA, Baerends EJ (2000) *J Chem Phys* 112:1344–1352
140. Gritsenko O, Baerends EJ (2004) *J Chem Phys* 121:655–660
141. Ziegler T, Krykunov M (2010) *J Chem Phys* 133:074104
142. Ziegler T, Seth M, Krykunov M, Autschbach J, Wang F (2009) *J Mol Struct Theochem* 914:106
143. Ziegler T, Seth M, Krykunov M, Autschbach J (2008) *J Chem Phys* 129:184114
144. Ziegler T, Seth M, Krykunov M, Autschbach J, Wang F (2009) *J Chem Phys* 130:154102
145. Cullen J, Krykunov M, Ziegler T (2011) *Chem Phys* doi: 10.1016/j.chemphys.2011.05.021
146. Hirata S, Head-Gordon SM (1999) *Chem Phys Lett* 314:291
147. Ballhausen CJ (1977) In: Segal GA (ed) *Semi-empirical methods of electronic calculation*, Part B. Plenum Press, New York

148. Lawley KP (1987) In: *Advances in chemical Physics*, vol 67. Wiley, New York
149. Koch H, Christiansen O, Jørgensen P, Sanchez de Merás AM, Helgaker T (1997) *J Chem Phys* 106:1808
150. Nooijen M, Bartlett RJ (1997) *J Chem Phys* 106:6441
151. Bartlett RJ, Stanton JF (2007) Applications of post-Hartree–Fock methods: a tutorial. In: Lipkowitz KB, Boyd DB (eds) *Reviews in computational chemistry*, vol 5. VCH, New York
152. Pierloot K (2011) *Int J Quant Chem* (Published online)
153. Special issue on electronic structure of metal complexes (2003) *Faraday Discuss* 124:1–455
154. Nooijen M (1999) *J Chem Phys* 111:10815
155. Nooijen M, Lotrich V (2000) *J Chem Phys* 111:494
156. Nakai H, Ohmori Y, Nakatsuji H (1991) *J Chem Phys* 95:8287
157. Johnson KH, Smith FC Jr (1971) *Chem Phys Lett* 10:219
158. Ziegler T, Rauk A, Baerends EJ (1976) *Chem Phys* 16:209
159. Stückel AC, Daul CA, Güdel HU (1997) *J Chem Phys* 107:4606
160. Neugebauer J, Baerends EJ, Nooijen M (2005) *J Phys Chem A* 109:1168
161. Fenske KF, Sweeney C (1964) *Inorg Chem* 3:1105
162. Viste A, Gray HB (1964) *Inorg Chem* 3:1113
163. Dahl JP, Johansen H (1968) *Theor Chim Acta* 11:8
164. Oleari L, De Michelis G, Di Sipio L (1966) *Mol Phys* 10:111
165. Brown RD, James BH, O'Dwyer MF, Roby KR (1967) *Chem Phys Lett* 1:459
166. Canadine RM, Hillier IH (1969) *J Chem Phys* 50:2984
167. Ballhausen CJ, Gray HB (1971) Electronic structures of metal complexes. In: Martell AE (ed) *Coordination chemistry*, vol 1. Van Nostrand Reinhold, New York
168. van Gisbergen SJA, Groeneveld JA, Rosa A, Snijders JG, Baerends EJ (1999) *J Phys Chem A* 103:6835
169. Boulet P, Chermette H, Daul CA, Gilardoni F, Weber J, Zuber G (2001) *J Phys Chem A* 105:885
170. Jitsuihiro S, Nakai H, Hada M, Nakatsuji H (1994) *J Chem Phys* 101:1029
171. Seth M, Krykunov M, Ziegler T, Autschbach J (2008) *J Chem Phys* 128:234102
172. Seth M, Ziegler T (2010) *Adv Inorg Chem* 62:41–109
173. Ziegler T, Autschbach J (2005) *J Chem Rev* 105:2695

Molecular Electronic Structures of Transition Metal
Complexes II

Mingos, D.M.P.; Day, P.; Dahl, J.P. (Eds.)

2012, XVI, 236 p., Hardcover

ISBN: 978-3-642-27377-3